Shear Strengthening of Reinforced Concrete T Beams with Hybrid Composite Plate (HCP)

Hadi Baghi[1], Joaquim A. O. Barros[2]

Abstract: This paper aims to evaluate the effectiveness of Hybrid Composite Plates (HCPs) technique for the shear strengthening of the Reinforced Concrete (RC) T cross section beams. HCP consists of a thin plate of Strain Hardening Cementitious Composite (SHCC) reinforced with Carbon Fiber Reinforced Polymer (CFRP) laminates. Two HCPs with different CFRP laminates percentage ($\rho_{fw} = 0.08\%$ and $\rho_{fw} = 0.14\%$) were adopted for the shear strengthening of the beams. The HCPs were bonded to substrate in two different ways. In the first case the HCPs were bonded using epoxy adhesive, while in the second case they were bonded using epoxy adhesive and fixed by mechanical anchors. The effectiveness of this technique was limited by the tensile strength of the concrete cover of the strengthened beams. Therefore in the second case, mechanical anchors prevented a premature debonding of the HCPs and a certain concrete confinement was applied in the zone of the beam to be strengthened, resulting in favorable effects in terms of shear strengthening.

Advanced FEM-based numerical simulation was performed by using a constitutive model, whose predictive performance was demonstrated by simulating the experimental tests carried out. After demonstration the good predictive performance of the numerical model, a parametric study was carried out to study the influence of shear reinforcement ratio, as well as the influence of thickness of the HCPs on the beam's load carrying capacity.

Keywords: Hybrid Composite Plate; CFRP laminates; Shear strengthening; Mechanical anchors; Numerical simulation; Finite Element Method.

[1] PhD, ISISE, Department of Civil Engineering, University of Minho, Guimarães, Portugal, (corresponding author) e-mail: hadibaghi@gmail.com.
[2] Full Professor, ISISE, Department of Civil Engineering, University of Minho, Guimarães, Portugal, e-mail: barros@civil.uminho.pt.

Introduction:

The strengthening or retrofitting of existing reinforced concrete (RC) structures to resist higher or different loading conditions, to attend for construction deficiencies, or to increase the ductility of their behavior has been accomplished using different materials and techniques. Bonding of thin steel plates (Abdel-Jaber et al. 2003), shotcrete jacketing (Tsonos 2010; Soleimani and Banthia 2012), and application of fiber reinforced polymer (FRP) by using externally bonded reinforcement (EBR) (Khalifa et al. 1998) or near surface mounted (NSM) (De Lorenzis and Nanni 2001; Rezazadeh et al. 2014) are some techniques that have been used as common retrofitting/strengthening techniques. Among the aforementioned techniques, application of the FRP material has been extensively studied due to high strength and stiffness-to-weight ratios. However, surface preparation, premature debonding of the FRP sheets and lack of protection against vandalism and fire are some disadvantages of this technique. Based on the results reported in De Lorenzis and Nanni (2001), Rizzo and De Lorenzis (2009), and Dias and Barros (2010), debonding of the FRP in the EBR technique and debonding with concrete fracture in the NSM technique (Bianco et al. 2009) avoid the full exploitation of the strengthening potentialities of the FRP materials. This is due to relatively low tensile strength of concrete cover that limits the bonding force between concrete and FRP (Chaallal et al. 2011). It was also observed that the effectiveness of the EBR and NSM techniques has been decreased with the increase of the percentage of steel stirrups (Chaallal et al. 2011; Mofidi and Chaallal 2011).

The use of anchor systems can prevent or delay this type of failure mode (Khalifa and Nanni 2000; De Lorenzis and Nanni 2001; Napoli et al. 2010; Mofidi and Chaallal 2011; Sena-Cruz et al. 2012), however the application of these systems requires extra time and costs, and can be susceptible to vandalism acts and the detrimental effect of environmental agents, since in general they are made of metallic materials. Special CFRP laminates, capable of being fixed with anchor devices without premature local rupture in the anchor zones, have been proposed, but these composite system are more expensive than current CFRP systems (Coelho et al. 2012; Sena-Cruz et al. 2012).

Strain Hardening Cementitious Composite (SHCC) can be support material for the FRP reinforcements in order to constitute an effective strengthening solution that can be fixed to concrete structures with anchorage systems. Recently, Hybrid Composite Plates (HCPs) have been used to increase the load carrying capacity, energy dissipation, hysteretic response (Esmaeeli et al. 2015), and ductility behavior of the RC elements. HCP is a thin layer of SHCC that is reinforced by CFRP laminates (Baghi et al. 2015), sheets (Anwar et al. 2009; Esmaeeli et al. 2013a). Due to the excellent bond conditions between SHCC plate and CFRP laminates/sheet, these reinforcements provide the necessary tensile strength capacity to the HCP. Moreover, the high post-cracking tensile deformability and resistance of SHCC avoid the occurrence of premature fracture failure of this cement composite in the stress transfer process between these two materials when the HCP is crossed by a shear crack (Baghi et al. 2015). The effectiveness of this technique is limited by tensile strength of the concrete substrate of the RC beams. Since, for a higher mobilization of the strengthening potentialities of this technique, the HCPs should be not only bonded to the substrate with an adhesive but also fixed with mechanical anchors (Esmaeeli et al. 2014). Besides the contribution of the SHCC for the strengthening efficiency of HCPs, the SHCC also assures some protection to the CFRP laminates and adhesive with respect to accidental actions, such as vandalism, aggressive environmental conditions, and fire.

In this work, the effectiveness of the HCPs with different shear percentage of the CFRP laminates (ρ_{fw}) and mechanical anchors is assessed experimentally. For this purpose, seven T cross section beams were tested, composed of one control beam, and six strengthened beams in shear with three different techniques: i) NSM-CFRP laminates, ii) SHCC plates, and iii) HCPs. In the last series, HCPs had different shear percentage of CFRP laminates ($\rho_{fw} = 0.08\%$ and $\rho_{fw} = 0.14\%$). The CFRP shear strengthening percentage, ρ_{fw} , is defined by the following equation (Eq. 1):

$$\rho_{fw} = \frac{2 a_f b_f}{b_w s_f \sin\theta_f} \tag{1}$$

where b_w = 180 mm is width of the beam's cross section, a_f = 1.4 mm and b_f = 10 mm are the dimensions of the NSM CFRP laminate cross section, s_f and θ_f represent the spacing and inclination of these laminates, respectively.

The HCPs were bonded to substrate in two different ways. In the first case, the HCPs were bonded using epoxy adhesive, while in the second case they were bonded using epoxy adhesive and fixed by mechanical anchors. The experimental program is detailed and the obtained results are presented and discussed.

Advanced numerical simulations were carried out by using a multi-directional fixed smeared crack model available in FEMIX computer program that includes a crack shear softening law to simulate the crack shear stress transfer degradation with the crack widening (Sena-Cruz et al. 2007). The values of the parameters that define this law were calibrated by simulating the tested beams and considering the properties obtained in the experimental programs for the characterization of the relevant properties of the used materials. By using this numerical model, a parametric study was carried out to evaluate the effectiveness of the shear strengthening ratio, as well as the influence of the thickness of the HCPs on the load carrying capacity of the strengthened beams.

Research Significance:

An experimental program with seven T cross section RC beams was executed in order to demonstrate the effectiveness of the Hybrid Composite Plates for the shear strengthening. The new technique aims to overcoming shortcomings of the EBR and NSM techniques such as: debonding of the FRP, lack of protection (vandalism and fire), and stress concentration caused by anchorage devices when used for avoiding the premature debonding of the FRP. The application of the HCPs with mechanical anchors was also effective in terms of residual load carrying capacity after peak load due to the excellent bond conditions between SHCC and CFRP laminates.

Experimental Program:

Test Program

Figure 1 presents the T cross section of the tested beams. The reinforcement systems were designed to assure shear failure mode for all the tested beams. The design methodologies were the same adopted elsewhere (Dias 2008). As shown in Fig. 1, to localize the shear failure in only one of the shear spans, a three point load configuration of a distinct length of the beam shear spans was selected. The length of the monitored shear span (L_i) was 2.5 times the effective depth of beam, which is the minimum recommendable value for assuring a negligible arch effect. To avoid shear failure in the other span a relatively high percentage of steel stirrups ($\phi 6@75$) was applied in this span (L_r). The characteristics of the beams are presented in Table 1. The C-R was a reference beam without any type of shear reinforcement and strengthening throughout the L_i shear span. The NSM-3L45 was a beam without steel stirrups in L_i span and was strengthened according to the NSM technique with 3 inclined CFRP laminates ($\theta = 45^\circ$) in each lateral face of L_i span, with a space (s_f) of 275 mm. The SP was a beam strengthened with SHCC plates to study the effectiveness of these plates for the shear strengthening. Each plate had overall dimension and weigh of 800×300×20 mm^3 and 8.6 kg, respectively. The SHCC plates were bonded to concrete substrate by using epoxy adhesive (S&P 220 supplied by clever Reinforcement Company). By applying the SHCC plates to the lateral faces of the beam the weight and width of beams' cross section became, respectively, 5% and 22%, larger than the corresponding one of the control beam (C-R).

As mentioned in the literature, the arrangement consisting of laminates at 45° is the most effective in terms of shear strengthening of the RC beams (De Lorenzis and Nanni 2001; Dias and Barros 2010). Therefore, this arrangement was selected in this experimental program. The SP-3L45 and SP-5L45 beams were strengthened by applying the HCPs in each lateral face of the L_i span by using epoxy adhesive. As shown in Fig. 2, the HCP is a 20 mm thick SHCC plate that was reinforced with three or five inclined CFRP laminates, spaced at 275 mm (SP-3L45 series) and 157 mm (SP-5L45 series).

In order to fully explore the shear strengthening potentialities of the HCPs, the HCPs in the SP-3L45-B and SP-5L45-B beams were not only bonded to lateral faces of their corresponding beams by using epoxy adhesive, but also fixed to the beam with 12 bolts of 10 mm diameter, according to the configuration presented in Fig. 3. The application of these mechanical anchors aims to prevent a premature debonding of the HCPs and to introduce a certain concrete confinement in the zone of the beam to be strengthened.

Material Properties

The concrete compressive strength was evaluated at the age when the beams were tested (45 days) by executing direct compression tests with cylinders of 150 mm diameter and 300 mm height according to EN-206-1 (de Normalisation 2000). The values of tensile properties of the steel bars were obtained from uniaxial tensile tests executed according to EN10002-1 recommendations (ISO 1990). The tensile property of the CFRP laminates was characterized by executing uniaxial tensile tests according to the recommendations of ISO 527-5 (European Standard 1997).

The SHCC is composed of a cementitious mortar reinforced with 2% in volume of short discrete polyvinyl alcohol (PVA) fibers of 40 μm diameter and 8 mm length. The average tensile stress at crack initiation and average tensile strength of the SHCC were 2.5 MPa and 3.4 MPa, respectively. More details on the preparation and testing the SHCC can be found elsewhere (Esmaeeli et al. 2012; Esmaeeli et al. 2013b). Tables 2 and 3 include the average values obtained from the experimental programs for the assessment of the relevant properties of concrete, CFRP laminates, SHCC, and steel bars.

Strengthening Techniques

Three different strengthening techniques were used in this study: i) NSM CFRP laminates, ii) SHCC plates, and iii) HCPs. The CFRP laminates were applied to the NSM-3L45 beam according to the NSM technique described in Dias and Barros (2010). The slits opened on the lateral faces of the RC beam for the installation of the CFRP laminates had a width and depth of about 5 mm and 15 mm, respectively.

For preparing the HCP, the CFRP laminates were applied into the SHCC plates following a procedure similar to the ones adopted for the RC beam. However, in this case the slits on the SHCC plates had a width and depth of about 4 mm and 11 mm, respectively. The HCPs were applied to their corresponding beams 7 days after the application of the CFRP laminates in order to guarantee a proper curing of the adhesive.

The SHCC/HCPs were applied to the lateral faces of the concrete beams by the following procedures:

1) A 1-2 mm roughness with sandblast was executed in the concrete substrate to improve the bond conditions between SHCC/HCPs and concrete beams;

2) In SP-3L45-B and SP-5L45-B beams, twelve holes were drilled with a diameter of 12 mm (Fig. 3) based on the suggestion of Li (1998) and Esmaeeli et al. (2014);

3) An epoxy adhesive (S&P220) layer of a thickness of about 1 mm was homogenously applied in the surfaces of the concrete beam and of the SHCC/HCPs that will be in contact;

4) In SP-3L45 and SP-5L45 beams mechanical clamps were used to maintain the SHCC/HPCs pressed against the lateral surfaces of the beam;

5) In the SP-3L45-B and SP-5L45-B beams the HCPs were fixed to the concrete substrate of these beams with 12 bolts and nuts (Fig. 3), by applying a torque of 20 N.m in the nuts on both sides of the beams. More information about these strengthening techniques can be found in Baghi (2015).

The C-R beam exhibited an incipient shear failure at support cross section due to a deficient execution of the anchorage length of the longitudinal reinforcement. Hence, to improve the anchorage conditions of the longitudinal reinforcement of the other beams, and avoid concrete spalling at the beam support section, a strengthening system based on the use of longitudinal NSM CFRP laminates of 1.4×20 mm^2 cross section and with a total length of 400 mm was applied on the bottom face of the beams, as illustrated in Fig. 4a.

Test Setup and Monitoring System

The load was applied by using a servo closed loop control equipment, taking the signal read in the displacement transducer (LVDT) of the servo-actuator to control the test at a deflection rate of 0.01 mm/s. The deflections of the beams at loaded section and at mid-span were measured by two LVDTs that were supported on an aluminum bar fixed at the alignments of the supports of the beams (Fig. 4a). With the purpose of obtaining the strain variation in the laminates, strain gauges were bonded to the CFRP laminates according to the arrangement represented in Fig. 4b.

Results of the tested beams

The relationships between force and deflection of the tested beams are presented in Fig. 5a. The SP-3L45, SP-3L45-B, and SP-5L45-B beams presented higher load carrying capacity compared to the other beams, which shows the effectiveness of the HCPs for the shear strengthening. The loaded section deflection at peak load of the SP-5L45-B beam was around 1.1 and 1.3 times higher than the corresponding deflection of the NSM-3L45 and SP beams, respectively. From the obtained results the $\Delta F_{\max} / F_{\max}^{SP} = (F_{\max} - F_{\max}^{SP}) / F_{\max}^{SP}$ ratio was evaluated, and the values are indicated in Table 4, where $F_{\max}^{SP}$ and $F_{\max}$ are the maximum load capacity of the beam strengthened with SHCC plates and of the other shear strengthened beams, respectively. For deflections higher than the one corresponding to the formation of the first shear crack in the NSM-3L45 (1.8 mm) and SP (2.5 mm) beams, it was calculated the $\Delta F^{NSM-3L45} / F^{NSM-3L45}$ and $\Delta F^{SP} / F^{SP}$ ratios, respectively, where $\Delta F^{NSM-3L45}$ and ΔF^{SP} is the increase of the load provided by HCPs ($\Delta F^{NSM-3L45} = F - F^{NSM-3L45}$, $\Delta F^{SP} = F - F^{SP}$), being $F^{NSM-3L45}$ and F^{SP} the load capacity of the beam strengthened with NSM CFRP laminates and SHCC plates, respectively, and F is the corresponding load capacity (for the same deflection) of the other strengthened beams with HCPs. These ratios were calculated up to $3\Delta_u^{SP}$ of the SP beam, where Δ_u^{SP} is the deflection corresponding to the maximum load of the SP beam.

As shown in Figs. 5b and 5c, the load of the SP-5L45-B and SP-3L45-B beams at deflection of about 15 mm is around 125% and 100% higher than the load of the NSM-3L45 and SP beams, respectively. These results show the effectiveness of the HCPs and also of the mechanical anchors in terms of post peak load carrying and deformability capacity. In fact, apart SP-5L45 beam, the post-peak performance of the beams shear strengthened with HCPs was much higher than the performance of the NSM-3L45 and SP beams.

By comparing the results of the strengthened beams with HCPs (Fig. 5b and Table 3) with those determined in the SP beam ($\Delta F_{\max} / F_{\max}^{SP}$) it is verified that the CFRP laminates contributed for the higher shear strengthening effectiveness of HCPs, since the laminates avoided the degeneration of the micro-cracks in the SHCC plates on macro-cracks, which had also a positive effect in terms of the stiffness preservation of the beam. The following sections provide a detailed analysis of the results for individual tested beams.

C-R beam

The C-R beam had no steel stirrups in the L_i span and any type of strengthening intervention. At a load of about 100 kN, two cracks became visible. One crack initiated at the support section (splitting crack), and the other one formed at the center of the shear span (Fig. 6a). By increasing the load, the cracks widened and propagated up to load of 214 kN and failure occurred at the support section of the beam (Fig. 6b). This failure mode was not expected and was caused by a deficient execution of the anchorage length of the longitudinal reinforcement. More information about this beam can be found in Baghi et al. (2015).

SP beam

The SP beam was strengthened with two 800×300×20 mm^3 SHCC plates that were bonded to each lateral face in L_i span by using epoxy adhesive (Fig. 4a). The first shear crack became visible by spraying oil (WD-40) on the surface of the SHCC plate (Fig. 6c). This shear crack formed at a load level of about 230 kN for a deflection of 2.6 mm. In this stage, the load was maintained almost constant up to deflection of around 3.5 mm, with the widening of this shear crack and the formation and propagation of some new cracks near the major shear crack. After that, the load started increasing due to the propagation of the shear failure crack through the flange of the beam towards the loaded area, and collapse occurred at a load level of about 255 kN and a deflection of 5.0 mm (Fig. 6d). This beam presented a brittle behavior, with an abrupt load decay at the post peak. As indicated in the previous section, the reinforcement mechanisms of fibers that were used in the SHCC (40 µm diameter and 8 mm length) were not able to absorb in a stable way the huge amount of energy released in the formation process of critical shear cracks, which justifies the brittle behavior of this beam in the post peak stage.

NSM-3L45 beam

The NSM-3L45 beam was strengthened with three inclined (45°) CFRP laminates in each lateral face of monitored shear span, spaced at 275 mm (Fig. 4). The CFRP shear strengthening percentage of this beam was $\rho_{fw} = 0.08\%$. The first shear crack became visible at around 350 mm from the support section (between laminates number 1 and 2, ellipse in Fig. 6e), at a load level of about 173 kN.

As reported in Bianco et al. (2011), the failure mode of a NSM CFRP laminate subjected to an imposed end slip can be categorized into four groups: a) debonding, b) tensile rupture of laminate, c) concrete semi-pyramid tensile fracture, and d) a mixed shallow semi-pyramid plus debonding failure mode (Fig. 7). These modes of failure are dependent on the relative mechanical and geometric properties of the materials involved. When principal tensile stresses transferred to the surrounding concrete attain its tensile strength, concrete fractures along a surface, envelope of the compression isostatics, whose shape can be assumed as a semi-cone (Bianco et al. 2010) or a semi-pyramid (Bianco et al. 2014). As shown in Fig. 6e by a circle, by increasing the load, some cracks formed around the laminate number 2, and the aforementioned mixed failure mode occurred in this laminate. Due to the quite short bond transfer length of the other two laminates, they did marginal contribution for the ultimate shear capacity of this beam. The laminate number 2 failed at a load and a deflection of about 275 kN and 4.1 mm, respectively, and the load was decreased of about 7%. After that, the load started increasing due to propagation of the shear crack through the flange of the beam towards the load area. An ultimate load of 291 kN was achieved at a deflection of 5.2 mm. As shown in Fig 5a, after an abrupt load decay, the load was stabilized at a load level of about 100 kN (32% of maximum load), which almost corresponds to the shear resistance assured by the longitudinal bars due to dowel effect, obtained according to the CEB-FIP MC (2010).

Due to the crack pattern (Fig. 6f), the highest longitudinal strain in the CFRP laminates was recorded in the SG2 (Fig. 4b) positioned almost coinciding with the shear failure crack, and was approximately 1.04%, which corresponds to 63% of the ultimate strain of the CFRP laminate. Figure 8 represents the relationship between applied load and strain in the SGs where the maximum CFRP laminate strain was registered in the strengthened beams. Up to the formation of the shear crack, the maximum strain increased almost linearly with the applied load, but did not exceed the strain value of 0.01%, demonstrating that these CFRP laminates had marginal shear strengthening contribution during this stage, as expected. However, at the formation of the shear failure crack an abrupt increase of strain occurred, more pronouncedly in the NSM-3L45 beam. This strain value and all those herein reported are not necessarily the maximum values, since they are dependent on the relative position of the SGs with respect to the shear cracks.

SP-3L45 beam

The SP-3L45 beam was strengthened with HCPs bonded to each lateral face in the L_i span using epoxy adhesive. As shown in Fig. 2a, the HCPs formed by the SHCC plates reinforced with three inclined CFRP laminates, spaced at 275 mm. The inclined lines in Fig. 8a show the position of the CFRP laminates.

The first shear crack formed at a load level of about 220 kN between laminates number 1 and 2, almost in the same location of the first shear crack in the NSM-3L45 beam. By increasing the load, several micro-cracks formed on the surface of the HCPs (Fig. 9a). The beam failed at a load of about 367 kN and a deflection of 5.5 mm. The failure of the beam was governed by the detachment of HCPs (Fig. 9b). As mentioned, the effectiveness of this technique was limited by the tensile strength of the concrete cover, as shown in Fig. 9b by an ellipse, at failure load, part of concrete cover was attached to the HCPs and local detachment occurred. After local detachment, the load was stabilized at a level of 42% of the maximum load (155 kN). This load level was higher than the load of the previous beam (NSM-3L45), since HCPs had connection in the other parts, Fig. 9c shows the local detachment of HCPs. The HCPs caused an increase in the load carrying capacity (44%) and its corresponding deflection (10%), when compared to the effect of the SHCC plates in the SP beam. The highest longitudinal strain in the CFRP laminates was recorded by the SG1 (Fig. 4b), and was approximately 0.41%, which corresponds to 25% of the ultimate strain of the CFRP laminate. The detachment of the HCPs justifies the relatively low collaboration of the CFRP laminates for the shear strengthening, demonstrated by the relatively small maximum strain registered (Fig. 8).

SP-3L45-B beam

The SP-3L45-B beam was identical to SP-3L45 beam, except that the HCPs were bonded using epoxy adhesive and fixed by 12 through bolts and nuts. A torque of 20 N.m was applied to tighten the nuts on both sides of the beam. Figures 3a and 3c show the position of the bolts and the CFRP laminates.

The first shear crack was detected at a load level of about 246 kN in the same position of the first crack in the SP-3L45 beam (between laminates number 1 and 2). By increasing the load, this crack widened and propagated. Figure 9d shows the crack pattern of this beam at failure load. At the load of 363 kN and a deflection of 6.2 mm the major shear crack was opened, with an abrupt load decay at peak load. After this abrupt load decay, the resisting load was almost maintained, at a load level of about 52% of maximum load (190 kN) up to the end of the test (a deflection of about 16 mm). The anchors contributed for the higher shear strengthening effectiveness of the HCPs in the post peak stage of the beam, avoiding the detachment of the HCPs. The deflection at maximum load of this beam was 13% and 24% higher than the deflection at maximum load of SP-3L45 and SP beams, respectively.

As shown in Fig. 9d, the laminate number 1 was torn off. However, since the SG3 did not function properly during the test, the highest longitudinal strain was recorded in the SG1 (Fig. 4b), and was approximately 0.69%, which corresponds to 42% of the ultimate strain of the CFRP laminate (Fig. 8).

SP-5L45 beam

The SP-5L45 beam was strengthened with HCPs reinforced with five CFRP laminates ($\rho_{fw} = 0.14\%$), spaced at 157 mm (Fig. 2b). The first flexural-shear crack formed at a load level of 166 kN. By increasing the load, several micro-cracks formed on the surface of the HCPs. The crack pattern in this beam presents much more cracks than in the other two previous beams, which is assumed to be caused by the higher percentage of CFRP laminates. The failure of this beam was premature debonding of adhesive at the load of 306 kN and a deflection of 5.1 mm. After an abrupt load decay, the load was stabilized at a load level of about 30% of the maximum load (dowel resistance of the longitudinal bars). The crack pattern of HCPs of this beam at failure load is shown in Fig. 9e. Due to the premature debonding of adhesive, no shear failure crack was visible on the surface of the HCPs, which indicates that the NSM CFRP laminates were not mobilized effectively. The highest tensile strain was recorded by the SG1 (Fig. 4b), and was approximately 0.33%, which corresponds to only 20% of the ultimate strain of the CFRP laminate (Fig. 8).

SP-5L45-B beam

In SP-5L45-B beam the HCPs were bonded to the lateral faces of the beam using epoxy adhesive and applying 12 through bolts and nuts (Fig. 3b), like the procedure adopted in the SP-3L45-B beam. The first shear crack was detected at a load of about 220 kN, intersecting the laminate number 4 (Fig. 9f). The failure of this beam occurred at a load of 364 kN and a deflection of 6.3 mm. The crack pattern of the HCPs presents much more shear and flexural-shear cracks, whose energy in their formation, as well as the resistance of the HCPs to the propagation of the shear failure crack have contributed for the significant increase in terms of ductility registered in this beam. In the SP-5L45-B beam, the reinforcement effectiveness of the CFRP laminates avoided the degeneration of the micro cracks into macro-shear failure crack on the SHCC, and the mechanical anchors prevented the premature detachment of the HCPs, and the failure was localized at the web-flange zone of the beam (marked with an ellipse in Fig. 9f). Since a strengthening discontinuity existed in this web-flange transition zone, and considering that no internal stirrups were available to offer resistance to the propagation of this type failure crack, the beams strengthened with HCPs fixed with adhesive and anchors could not exceed the maximum load attained by the SP-5L45-B beam, regardless the percentage of the CFRP laminates and number of the bolts used. However, as it is visible in the post-peak stage of this beam, the load decay was much smoother, and the residual load carrying capacity of this beam (55% of the maximum load) was much higher than the one registered in the previous beams, due to the larger fracture surface mobilized in the failure mode of the SP-5L45-B beam.

The maximum longitudinal strain measured in the CFRP laminates (SG3, Fig. 4b) was 1.12% (Fig. 8), which corresponds to 68% of the ultimate strain of the CFRP laminate, that is higher than the maximum strain recorded in the NSM-3L45 beam. This result shows the effectiveness of the mechanical anchors to avoid premature detachment of the HCPs and to assure higher collaboration of the CFRP laminates for the shear strengthening.

Energy Evaluation:

Toughness indicator, as a measure of the energy absorption capacity, was obtained for each beam by determining the area behind the force *vs.* loaded section deflection curve up to three times Δ_u^{SP} of the SP beam, whose values are indicated in Table 5.

The SP-5L45 beam, which failure was governed by debonding of adhesive, shows the minimum toughness amongst the strengthened beams with HCPs. In the post-peak stage of the SP-3L45-B and SP-5L45-B beams, the load decay was much smoother (Fig. 5a), and the residual load carrying capacity of these beams was much higher than the one registered in the corresponding beams without mechanical anchors. The toughness of these beams was about 5% and 68% higher than the one of the corresponding beams without mechanical anchors (SP-3L45 and SP-5L45), respectively. The toughness of the SP-5L45-B beam was around 10% higher than the one corresponding to the SP-3L45-B beam. Therefore, by increasing the number of CFRP laminates and using mechanical anchors for applying the HCPs to the RC beams is an effective strategy for enhancing the energy absorption capacity of the strengthened beam in its post-peak stage. The mechanical anchors prevented a premature debonding of the HCPs, and applied a certain concrete confinement in the zone of the beam to be strengthened, resulting in favorable effects in terms of shear strengthening.

Numerical Simulations:

The three dimensional multi-directional fixed smeared crack model described in detailed in Ventura-Gouveia (2011), implemented in the FEM-based computer program, FEMIX, was used in the numerical simulations carried out in this work.

To simulate the crack initiation and the fracture mode I propagation of plain concrete and SHCC, the tri-linear tension-softening diagram presented in Fig. 10 was adopted (Sena-Cruz 2004), which is defined by the parameters α_i and ξ_i, relating stress with strain at the transitions between the linear segments that compose this diagram. The ultimate crack strain, $\varepsilon_{n,u}^{cr}$, is defined as a function of the parameters α_i and ξ_i, the fracture energy, G_f^I, the tensile strength, $\sigma_{n,1}^{cr} = f_{ct}$, and the crack bandwidth, l_b. The values of the relevant quantities defining of this diagram are indicated in Tables 6 and 7 for plain concrete and SHCC, respectively. These tables also include the data necessary to define the shear-softening relationship that simulates the degradation of crack shear stress transfer after crack initiation (Ventura-Gouveia et al. 2008; Ventura-Gouveia 2011; Barros et al. 2013) presented in Fig. 11.

To simulate the fracture mode II modulus, a shear retention factor is used (Eq. 2):

$$D_{t_1}^{cr} = D_{t_2}^{cr} = \frac{\beta}{1-\beta} G_c \tag{2}$$

where G_c is the concrete elastic shear modulus and β is the shear retention factor. $D_{t_1}^{cr}$ and $D_{t_2}^{cr}$ represent the modulus correspondent to the sliding mode stiffness modulus in the $\hat{t}_1$ direction and the sliding mode stiffness modulus in the $\hat{t}_2$ direction, respectively (Fig. 12). The parameter β is defined as a constant value or as a function of the current crack normal strain, ε_n^{cr}, and of the ultimate crack normal strain, $\varepsilon_{n,u}^{cr}$, as follows (Eq. 3):

$$\beta = \left(1 - \frac{\varepsilon_n^{cr}}{\varepsilon_{n,u}^{cr}}\right)^{p_1} \tag{3}$$

When $P_1 = 1$ a linear decrease of β with the increase of ε_n^{cr} is assumed. Larger values of the exponent P_1 correspond to a more pronounced decrease of the β parameter. In structures governed by flexural failure modes, this strategy leads to simulations with good accuracy (Barros et al. 2011). Exceptions occur in structures that fail by the formation of a critical shear crack. To simulate accurately the deformational response and the crack pattern up to the failure of this type of structures, the adoption of a softening crack shear stress *versus* crack shear strain relationship was adopted to model the crack shear transfer in $\hat{t}_1$ and $\hat{t}_2$ direction.

The adopted crack shear diagram is represented in Fig. 11. The crack shear stress increases linearly until the crack shear strength is reached, $\tau_{t,p}^{cr}$, (first branch of the shear crack diagram), followed by a decrease in the shear residual strength (softening branch). This diagram is defined by Eq. 4:

$$\tau_t^{cr}\left(\gamma_t^{cr}\right)=\begin{cases} D_{t,1}\,\gamma_t^{cr} & 0<\gamma_t^{cr}\leq\gamma_{t,p}^{cr} \\ \tau_{t,p}^{cr}-\dfrac{\tau_{t,p}^{cr}}{\left(\gamma_{t,u}^{cr}-\gamma_{t,p}^{cr}\right)}\left(\gamma_t^{cr}-\gamma_{t,p}^{cr}\right) & \gamma_{t,p}^{cr}<\gamma_t^{cr}\leq\gamma_{t,u}^{cr} \\ 0 & \gamma_t^{cr}>\gamma_{t,u}^{cr} \end{cases} \tag{4}$$

The initial shear fracture modulus, $D_{t,1}^{cr}$, is defined by Eq. 2 ($D_{t_1}^{cr}$ is replaced by $D_{t,1}^{cr}$) by assuming for β a constant value in the range $]0,1[$. The peak crack shear strain, $\gamma_{t,p}^{cr}$, is obtained using the crack shear strength (from the input data), $\tau_{t,p}^{cr}$, and the crack shear modulus (Eq. 5):

$$\gamma_{t_1,p}^{cr}=\gamma_{t_2,p}^{cr}=\frac{\tau_{t,p}^{cr}}{D_{t,1}^{cr}} \tag{5}$$

The ultimate crack shear strain, $\gamma_{t,u}^{cr}$, depends on the crack shear strength, $\tau_{t,p}^{cr}$, on the shear fracture energy (mode II fracture energy), $G_{f,s}$, and on the crack bandwidth, l_b (Eq. 6):

$$\gamma_{t_1,u}^{cr}=\gamma_{t_2,u}^{cr}=\frac{2G_{f,s}}{\tau_{t,p}^{cr}l_b} \tag{6}$$

In this approach it is assumed that the crack bandwidth, used to assure that the results are independent of the mesh refinement (Rots 1988), is the same adopted for the fracture mode I. It is also assumed that the crack shear behavior in both t_1 and t_2 directions is simulated by the same constitutive law.

The crack mode II modulus of the first linear branch of the diagram is defined by Eq. 2, the second linear softening branch is defined by Eq. 7:

$$D_{t_1}^{cr}=D_{t_2}^{cr}=D_{t,2}^{cr}=-\frac{\tau_{t,p}^{cr}}{\gamma_{t,u}^{cr}-\gamma_{t,p}^{cr}} \tag{7}$$

and the crack shear modulus of the unloading and reloading branches is obtained from Eq. 8:

$$D_{t_1}^{cr}=D_{t_2}^{cr}=D_{t,3-4}^{cr}=\frac{\tau_{t,\max}^{cr}}{\gamma_{t,\max}^{cr}} \tag{8}$$

being $\gamma_{t,\max}^{cr}$ and $\tau_{t,\max}^{cr}$ the maximum crack shear strain already attained and the corresponding crack shear stress determined from the softening linear branch. Both components are stored to define the unloading/reloading branch (see Fig. 11).

In free - sliding status ($\left|\gamma_t^{cr}\right| > \left|\gamma_{t,u}^{cr}\right|$) the crack mode II stiffness modulus, $D_{t_1}^{cr} = D_{t_2}^{cr} = D_{t,5}^{cr}$, is null. To avoid numerical instabilities in the calculation of the stiffness matrix and in the calculation of the internal forces, when the crack shear status is free - sliding, a residual value is assigned to this term. A free - sliding status is assigned to the shear crack status when $\varepsilon_n^{cr} > \varepsilon_{n,u}^{cr}$ (Barros et al. 2013). More details of the remaining variables of this constitutive model can be found in Barros et al. (2013) and Ventura-Gouveia (2011).

The data for the shear softening diagram of plain concrete was determined by fitting as best as possible the force-deflection relationship registered in the control beam tested experimentally (C-R), while for the SHCC this data was obtained by simulating the SP beam. For the analysis of the remaining beams of the experimental program the values of the constitutive model applied to each intervening material were preserved constant. Figure 13 represents the finite element mesh adopted for the control beam (C-R). In the simulations, this finite element mesh was only altered in order to take into account the strengthening provided by CFRP laminates (NSM-3L45 beam), the SHCC plate (SP beam), and HCPs.

Only half of the full size beam was modeled, taking advantage of the symmetry of the beams in order to reduce the computational time of the numerical simulations. Serendipity 8 nodes solid elements with 2×2×2 Gauss-Legendre integration scheme were used for both the concrete and SHCC (three degrees-of-freedom per node). The steel stirrups, longitudinal steel bars and CFRP laminates were modeled with 3D embedded cables of 2 nodes (one degree-of-freedom per node), by using a 2 Gauss-Legendre integration scheme, and perfect bond to the surrounding medium was assumed. The bolts are modeled with 3D two-node truss elements, and the confinement effect locally induced on concrete by the torque of anchors was simulated by applying a temperature decrease of -25.5°C in these elements, evaluated according to the following equations (Eq. 9):

$$F = \frac{\tau}{r} \qquad F = \frac{20}{0.005} = 4000\ N \tag{9a}$$

$$\sigma = \frac{F}{A} \qquad \sigma = \frac{4000}{78.5} = 51 MPa \tag{9b}$$

$$\varepsilon = \frac{\sigma}{E} = T.\alpha \qquad \varepsilon = \frac{51}{200000} = T \times 10^{-5} \tag{9c}$$

where τ is torque (N.m), and r, A, and E are the radius, cross sectional area, and elasticity modulus of the bolt (5 mm, 78.5 mm^2, 200 GPa), respectively. In these equations T and α are the temperature variation and the coefficient of thermal expansion, respectively. The relation between applied torque and axial tension force fastener is presented in Fig. 14. More information about this formulation can be found in Baghi (2015).

An elasto-perfectly plastic model was adopted to simulate the tension and compression behavior of the steel reinforcements, whose fundamental information is indicated in Table 3. For modeling the NSM CFRP laminates, a linear elastic stress-strain relationship was adopted. The assumption of perfect bond between substrate and SHCC plates was assumed. Newton-Raphson Standard method was applied, and energy convergence tolerance of 10^{-4} was taken.

The experimental and the numerical relationships between the applied load and the deflection at the loaded section for the tested beams are compared in Fig. 15. The crack pattern of these beams at the end of the analysis is represented in Fig. 16. During the last not converged loading step, several cracks in the critical shear zone open completely (fracture energy is completely exhausted – red color), and since this abrupt crack propagation is restricted to the critical shear zone (which resembles what happened in the experimental tests), convergence was no more possible to be assured.

Figures 15 and 16 show that the numerical model is capable of predicting with high accuracy the load *vs.* deformational response of the beams, and to capture with a good precision the localization and profile of the failure cracks. These results confirm the capability of the developed model to simulate to behavior of RC beams failing in shear. For the beams strengthened with SHCC/HCP, the crack pattern is represented for the lateral surface of the concrete substrate, as well as for the SHCC/HCP. The higher load predicted for the SP-5L45 indicates that the assumed perfect bond conditions between HCPs and concrete substrate was not assured in this beam, pointing out that some deficiency was occurred in the bonding process, as already reported. The crack pattern of the beams strengthened with SHCC/HCP shows the tendency of the failure crack to propagate at the web-flange interface due to the discontinuity of beam's cross section stiffness and shear strengthening contribution of the SHCC/HCP.

Figure 17 also shows that the numerical simulations fit with good accuracy the strains measured in the NSM laminates, which means that the assumption of perfect bond between NSM laminates and surrounding SHCC is acceptable, at least in the design point of view for the serviceability and ultimate limit states.

Based on results, it can be concluded that the implementation of the shear softening diagram in the multi-directional fixed smeared crack model available in the FEMIX computer program is capable of predicting with high accuracy the deformational behavior, load carrying capacity, and crack patterns of structures failing in shear.

The applicability of this type of numerical simulations in real strengthening interventions requires the assessment of the concrete compressive strength from non-destructive (extraction of core samples) or non-invasive techniques (e.g. ultra-sonic). From the concrete compressive strength and using the recommendations of design codes, like CEB-FIP Model Code, the mode I fracture parameters can be determined. However, the evaluation of the mode II fracture parameters, like the ones required for defining the crack shear softening diagram, is still a challenging task. Nonetheless, based on experience of the authors, shear retention factor (β), crack shear strength ($\tau_{t,p}^{cr}$), and fracture energy mode II ($G_{f,s}$) for the normal concrete are between 0.4 to 0.6, 0.9 to 1.1, and 0.03 to 0.06, respectively. Parametric studies have also been carried out by Barros et al. (2013) and Breveglieri (2015) to investigate the influence of these parameters on the load carrying capacity and deflection performance of shear strengthened RC beams. Finally, there is also a database for the shear strengthening of RC beams (http://dabasum.civil.uminho.pt/) that can be useful for deriving the model parameters by simulating by inverse analysis the experimental tests included in this database.

Parametric Study:

The computer program, whose good predictive performance for the simulation of the behavior of the type of structures under consideration was confirmed in the previous section, was adopted to execute a parametric study to evaluate effectiveness of shear reinforcement ratio and also the thickness of the HCP on the load carrying capacity and failure mode of the beams strengthened with HCPs. The arrangement of the steel reinforcements, the material properties of concrete and SHCC, the support and load conditions, and the finite element mesh were the same ones adopted in the numerical simulations of the previous section.

Influence of Shear Reinforcement Ratio

Based on the results of the experimental program, the failure of the SP-5L45-B beam was localized at the web-flange zone, which avoided to exploit the full strengthening potential of these HCPs. Thus, to access the shear strengthening effectiveness of these HCPs in situations where a certain percentage of steel stirrups exists, two values for the reinforcement ratio of existing steel stirrups were considered: 2 ϕ6@300 mm (ρ_{sw} =0.10%) and 4 ϕ6@150 mm (ρ_{sw} =0.20%). The relationship between load and deflection at loaded section for the simulated beams are presented in Fig. 18. As mentioned in the introduction, the effectiveness of the EBR and NSM techniques has been decreased by increasing the percentage of steel stirrups. However, based on the results of the numerical simulation, in the HCPs technique the strengthening effectiveness has increased by increasing the percentage of existing steel stirrups. In these beams a critical diagonal shear crack was formed and beam failed at peak load without the occurrence of yield initiation of the longitudinal reinforcement.

Influence of thickness of SHCC panel

In this case, the influence of thickness of the HCPs on the load-deflection and stiffness was investigated. For this purpose, two other thicknesses of HCPs were assumed: 15 mm and 40 mm, the first one is lower and the last one is higher than the one corresponding to the thickness of the HCPs of the SP-5L45-B beam. To avoid the localization of the failure at web-flange zone, 2 steel stirrups $\phi 6@300$ (ρ_{sw} =0.10%) were added in the monitored shear span. The obtained results, depicted in Fig. 19, show that the thickness of the HCPs has a relatively small influence on the stiffness of the strengthened beams. However, by increasing the thickness of the HCPs the load carrying capacity and ultimate deflection have increased significantly. All simulated beams failed in shear.

Conclusions:

The effectiveness of Hybrid Composite Plates (HCPs) for the shear strengthening of reinforced concrete (RC) beams was investigated by carrying out an experimental program, which was complemented with FEM-based advanced numerical simulations. From the obtained results, the following conclusion can be drawn:

- The HCPs increased the shear capacity of the beams around 43% compared to the beam strengthened with SHCC plates.
- The strain hardening cement composites (SHCC) surrounding the carbon fiber reinforced polymer (CFRP) laminates has offered effective resistance to the degeneration of micro-cracks on macro-cracks.
- The effectiveness level of the HCP technique was limited by the tensile strength of the concrete substrate of the RC beams and maximum tensile strain in the CFRP laminates did not exceed 25% of the ultimate strain of these laminates. Therefore mechanical anchors were used to prevent this premature detachment.
- The load carrying capacity of the strengthened beams with HCP technique was limited by the shear strengthening discontinuity at the web-flange of the beam, since in these strengthened beams the failure crack propagated through this zone.

- The HCPs were capable of increasing not only the load carrying and deflection capacity, but also the post-peak resisting load, with favorable effects in terms of energy absorption capacity.
- The shear crack softening diagram available in the multi-directional fixed smeared crack model implemented in the FEMIX computer program, allowed to predict with high accuracy the load carrying capacity, crack patterns, strain in the CFRP laminates, and failure modes of the tested beams.
- The results of the parametric study show that by increasing the reinforcement ratio of existing steel stirrups, the strengthening effectiveness of the HCPs has increased, which is an extremely important attribute of this technique, since the opposite occurs with EBR and NSM techniques. The load carrying capacity and ultimate deflection of the beams have increased with the thickness of the HCPs.

ACKNOWLEDGMENTS

The study presented in this paper is a part of the research project titled "PrePam –Pre-fabricated thin panels by using advanced materials for structural rehabilitation" with reference number of PTDC/ECM/114511/2009 provided by FCT (Fundação para a Ciência e a Tecnologia). The first author acknowledges the research grant provided by this project. The authors also thank the collaboration of the following companies: Clever Reinforcement Iberica for providing the CFRP laminates and epoxy, Sika for the sand and adhesive, Grace for the superplasticizers, Dow Chemical Co. for viscous modifying agents, ENDESA Compostilla power station for the fly ash, and Casais for assisting in the execution of the beams.

References:

Abdel-Jaber, M. S., Walker, P.R., and Hutchinson, A.R. (2003). "Shear strengthening of reinforced concrete beams using different configurations of externally bonded carbon fiber reinforced plates." *Materials and Structures* 36: 291-301.

Anwar, A. M., Hattori, K., Ogata, H., and Ashraf, M. (2009). "Engineered Cementitious Composites for Repair of Initially Cracked Concrete Beams." *Asian Journal of Applied Sciences* 2(3): 223-231.

Baghi, H. (2015). The effectivness of SHCC-FRP panles of the shear resistance of RC beams, University of Minho, PhD Thesis.

Baghi, H., Barros, J.A.O., Rezazadeh, M., and Laranjeira, J., (2015), "Strengthening of Damaged Reinforced Concrete Beams with Hybrid Composite Plates", *Journal of Composites for Construction (ASCE)*. DOI: 10.1061/(ASCE)CC.1943-5614.0000601.

Barros, J.A.O., Costa, I. G., and Ventura Gouveia, A. (2011). "CFRP flexural and shear strengthening technique for RC beams: experimental and numerical research." *Advances in Structural Engineering Journal*, 14(3): 559-581.

Barros, J. A. O., Baghi, H., Dias, S.J.E., and Ventura-Gouveia. A. (2013). "A FEM-based model to predict the behaviour of RC beams shear strengthened according to the NSM technique." *Engineering Structures* 56: 1192–1206.

Bianco, V., Barros, J.A.O., and Monti, G. (2009). "Three dimensional mechanical model for simulating the NSM FRP strips shear strength contribution to RC beams." *Engineering Structures* 31(4): 815-826.

Bianco, V., Barros, J.A.O., and Monti, G. (2010). "New approach for modeling the contribution of NSM FRP strips for shear strengthening of RC beams." *ASCE Composites for Construction Journal* 14(1): 36-48.

Bianco, V., Monti, G., and Barros, J.A.O. (2011). "Theoretical model and computational procedure to evaluate the NSM FRP strips shear strength contribution to a RC beam." *ASCE Journal of Structural Engineering* 137(11).

Bianco, V., Monti, G., and Barros, J.A.O. (2014). "Design formula to evaluate the NSM FRP strips shear strength contribution to a RC beam." *Composites Part B: Engineering* 56: 960-971.

CEB-FIP model code 2010, first completed draft, 2010, Comité Euro-International du Béton, Lausanne, Switzerland.

Chaallal, O., Mofidi, A., Benmokrane, B., and Neale, K. (2011). "Embedded Through-Section FRP Rod Method for Shear Strengthening of RC Beams: Performance and Comparison with Existing Techniques." *Composites for Construction (ASCE)*, 19: 374-383.

Coelho, M., Fernandes, P., Sena-Cruz, J.M., and Barros, J.A.O. (2012). "Bond behavior between concrete and multi-directional CFRP laminates using the MF-EBR strengthening technique." *Advanced Materials Reasearch*: 1110-1115.

De Lorenzis, L., and Nanni, A. (2001). "Shear Strengthening of Reinforced Concrete Beams with Near-Surface Mounted Fiber-Reinforced Polymer Rods." *ACI Structural Journal* 98: 60-68.

de Normalisation, C. E. (2000). Concrete - Part 1: Specification, performance, production and conformity, EN206-1, CEN. : 69.

Dias, S.J.E., (2008). Experimental and analytical research on the shear strengthening of RC beams by means of CFRP laminates applied according to the NSM technique. University of Minho, PhD thesis, (in Portuguese).

Dias, S. J. E., and Barros, J.A.O. (2010). "Performance of reinforced concrete T beams strengthened in shear with NSM CFRP laminates." *Engineering Structures*, 32: 373-384.

Esmaeeli, E., Barros, J., and Mastali, M. (2012). Effects of curing conditions on crack bridging response of PVA reinforced cementitious matrix. 8th RILEM international symposium on fibre reinforced concrete: challenges and opportunities (BEFIB2012). Guimaraes, Portugal.

Esmaeeli, E., Barros, J.A.O., and Baghi, H. (2013a). Hybrid Composite Plates (HCP) for Shear Strengthening of RC Beams. FRPRCS11. University of Minho, Guimarães, Portugal.

Esmaeeli, E., Barros, J.A.O., Baghi, H., and Sena-Cruz, J. (2014). Development of Hybrid Composite Plate (HCP) for the Repair and Strengthening of RC Elements. 3rd International RILEM Conference on Strain Hardening Cementitious Composites (SHCC3-Delft). Delft University.

Esmaeeli, E., Barros, J.A.O., Sena-Cruz, J., Varum, H., and Melo, J. (2015). "Assessment of the efficiency of prefabricated hybrid composite plates (HCPs) for retrofitting of damaged interior RC beam–column joints." *Composite Structures*, (119): 24-37.

Esmaeeli, E., Manning, E., and Barros, J.A.O. (2013b). "Strain hardening fibre reinforced cement composites for the flexural strengthening of masonry elements of ancient structures." *Construction and Building Materials*, 38: 1010-1021.

European Standard (1997). Plastics - determination of tensile properties Part 5: Test conditions for unidirectional fibre-reinforced plastic composites. ISO 527-5, Geneva (Switzerland): International Organization for Standardization (ISO).

ISO, E. (1990). Metallic materials Tensile testing-Part 1: Method of test (at ambient temperature), Brussels: European committee for standardization (cen).

Khalifa, A., Gold, W.J., Nanni, A., and Aziz, A. (1998). "Contribution of externally bonded FRP to shear capacity of RC flexural members." *Composites for Construction (ASCE)*, 2(4): 195-203.

Khalifa, A., and Nanni, A. (2000). "Improving shear capacity of existing RC T-section beams using CFRP composites." *Cement & concrete Composites*, 22: 165-174.

Li, V.C., "Engineered Cementitious Composites for Structural Applications. (1998) " *Materials in Civil Engineering* (ASCE), 10 (2): p. 66-69.

Mofidi, A., and Chaallal, O. (2011). "Shear Strengthening of RC Beams with EB FRP: Influencing Factors and Conceptual Debonding Model." *Composites for Construction (ASCE)*, 15: 62-74.

Napoli, A. M., F.; Martinelli, E.; Nanni, A.; and Realfonzo, R. (2010). "Modelling and Verification of Response of RC Slabs Strengthened in Flexure with Mechanically Fastened FRP Laminates." *Magazine of Concrete Research*, 62, 593-605.

Rezazadeh, M., Costa, I., and Barros, J. (2014). "Influence of prestress level on NSM CFRP laminates for the flexural strengthening of RC beams." *Composite Structures*, 116: 489-500.

Rizzo, A., and De Lorenzis, L. (2009). "Behaviour and capacity of RC beams strengthened in shear with NSM FRP reinforcement." *Construction and Building Materials*, 3(No.4): 1555-1567.

Rots, J. G. (1988). Computational modeling of concrete fracture. PhD Thesis, Delft University of Technology.

Sena-Cruz, J., Barros, J.A.O., Coelho, M., and Silva, L. (2012). "Efficiency of different techniques in flexural strengthening of RC beams under monotonic and fatigue loading." *Construction and Building Materials*, 29: 175-182.

Sena-Cruz, J. M. (2004). Strengthening of concrete structures with near-surface mounted CFRP laminate strips. PhD Thesis, University of Minho.

Sena-Cruz, J. M., Barros, J.A.O., Azevedo, A.F.M., and Ventura-Gouveia, A. (2007). Numerical simulation of the nonlinear behavior of RC beams strengthened with NSM CFRP strips. CMNE/CILAMCE Congress, FEUP, Porto, Portugal.

Soleimani, S. M., and Banthia, N. (2012). "Shear Strengthening of RC Beams Using Sprayed Glass Fiber Reinforced Polymer." *Advances in Civil Enginee*ring, 2012, Doi:10.1155/2012/635176.

Tsonos, A. D. (2010). "Performance enhancement of R/C building columns and beam–column joints through shotcrete jacketing." *Engineering Structures* 32: 726-740.

Ventura-Gouveia, A. (2011). Constitutive models for the material nonlinear analysis of concrete structures including time-dependent effects. PhD Thesis, University of Minho.

Ventura-Gouveia, A., Barros, J., Azevedo, A., and Sena-Cruz, J. (2008). Multi-fixed smeared 3d crack model to simulate the behavior of fiber reinforced concrete structures. CCC 2008 - Challenges for Civil Construction. Porto, Portugal.

LIST OF Figure CAPTIONS

Fig. 1 - Geometry and reinforcement arrangement of the concrete beams (dimensions in mm)

Fig. 2 – Position of the CFRP laminates inside of the SHCC plate a) SP-3L45 beam, b) SP-5L45 beam (dimensions in mm)

Fig. 3- Position of the CFRP laminates and mechanical anchors a) SP-3L45-B, b) SP-5L45-B, c) position of the bolts inside of the RC beams (dimensions in mm)

Fig. 4- Monitoring system- position of the: a) LVDTs; and b) strain gages in CFRP laminates (dimensions in mm)

Fig. 5- a) Force vs. deflection at the loaded-section, b) $\Delta F / F^{NSM-3L45}$ vs. deflection at the loaded-section for the beams strengthened with SHCC/HCPs, and c) $\Delta F / F^{SP}$ vs. deflection at the loaded-section for the beams strengthened with HCPs

Fig. 6 - Crack patterns and failure modes of the C-R, NSM-3L45, and SP beams

Fig. 7 - The mode of failure of an NSM CFRP laminate subjected to an imposed end slip

Fig. 8 - Force vs. strain in monitored laminates in SGs where the maximum strains were registered

Fig. 9 - Crack patterns and failure modes of the strengthened beams with HCPs

Fig. 10 - Trilinear stress-strain diagram to simulate the fracture mode I crack propagation

Fig. 11 - Diagrams to simulate the relationship between the crack shear stress and crack shear strain component, and possible shear crack statuses

Fig. 12 - Crack stress components, displacements and local coordinate system of the crack

Fig. 13 - Finite element mesh of the C-R beam (dimensions in mm)

Fig. 14 - The relation between applied torque to axial tension force fastener

Fig. 15 - Comparison between experimental and numerical force vs. deflection at the loaded section relationships

Fig. 16 - Crack patterns of the beams (in red color: crack completely open; in black color: crack in the opening process)

Fig. 17 - Comparison between experimental and numerical force vs. strains in the CFRP laminates

Fig. 18 – Influence of the reinforcement ratio of existing steel stirrups on the load carrying capacity of HCP strengthened beams

Fig. 19 – Influence of thickness of HCPs on the load carrying capacity and ultimate deflection

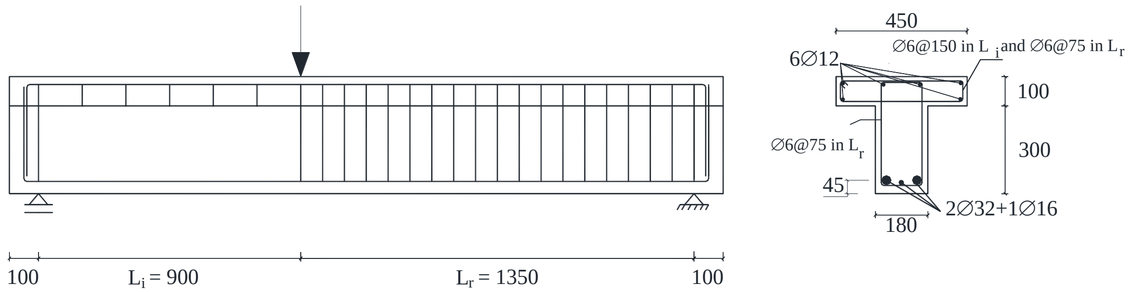

Fig. 1 - Geometry and reinforcement arrangement of the concrete beams (dimensions in mm)

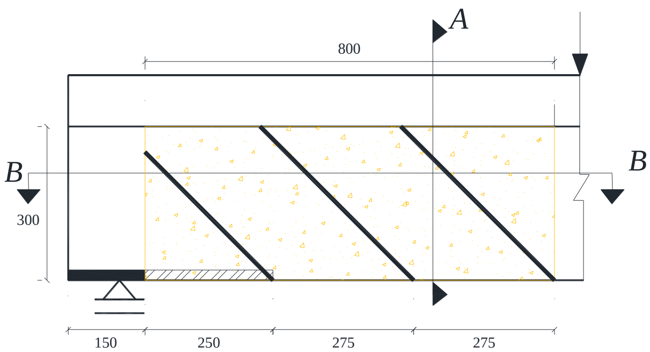

a) SHCC plate with three inclined CFRP laminates ($\rho_{fw} = 0.08\%$)

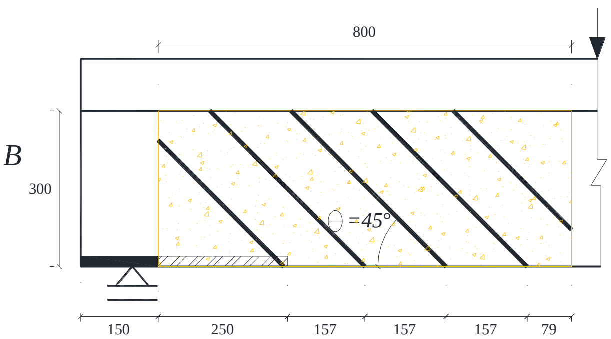

b) SHCC plate with five inclined CFRP laminates ($\rho_{fw} = 0.14\%$)

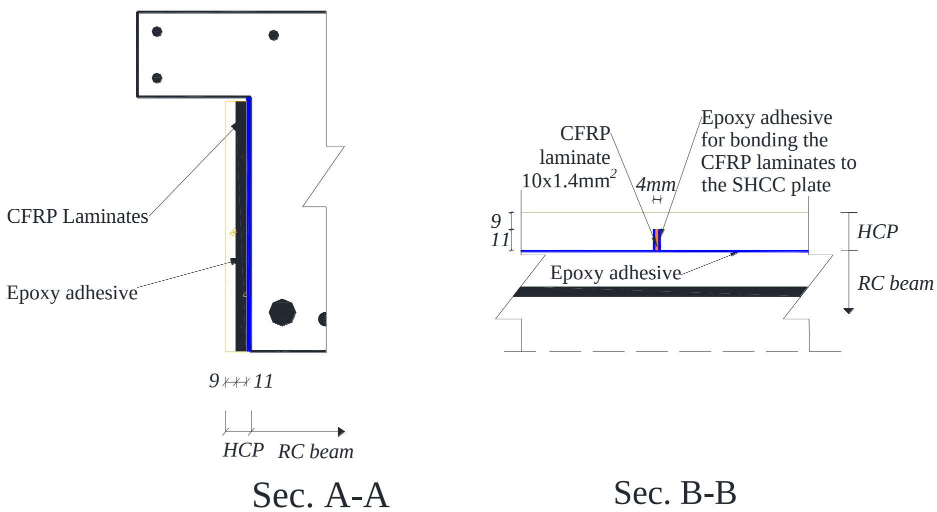

c) A section view of the strengthened beam with HCPs

Fig. 2 – Position of the CFRP laminates inside of the SHCC plate a) SP-3L45 beam, b) SP-5L45 beam (dimensions in mm)

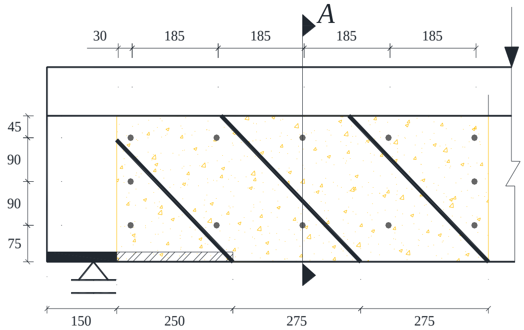

a) SHCC plate with three inclined CFRP laminates ($\rho_{fw} = 0.08\%$) and 12 anchors

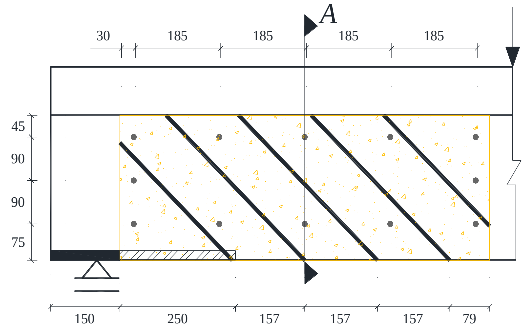

b) SHCC plate with five inclined CFRP laminates ($\rho_{fw} = 0.14\%$) and 12 anchors

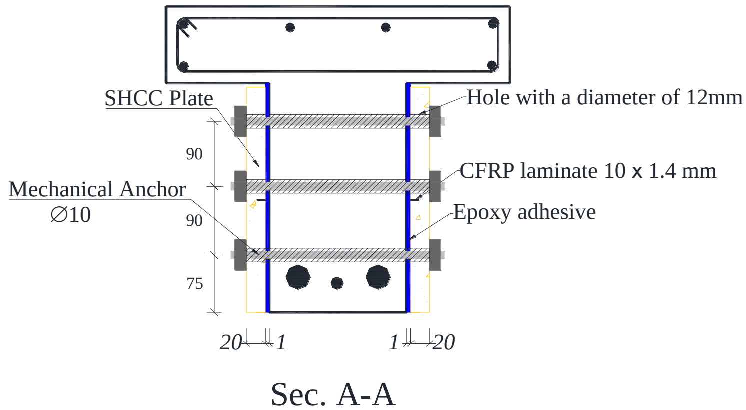

c) position of the bolts inside of the RC beams

Fig. 3- Position of the CFRP laminates and mechanical anchors a) SP-3L45-B, b) SP-5L45-B, c) position of the bolts inside of the RC beams (dimensions in mm)

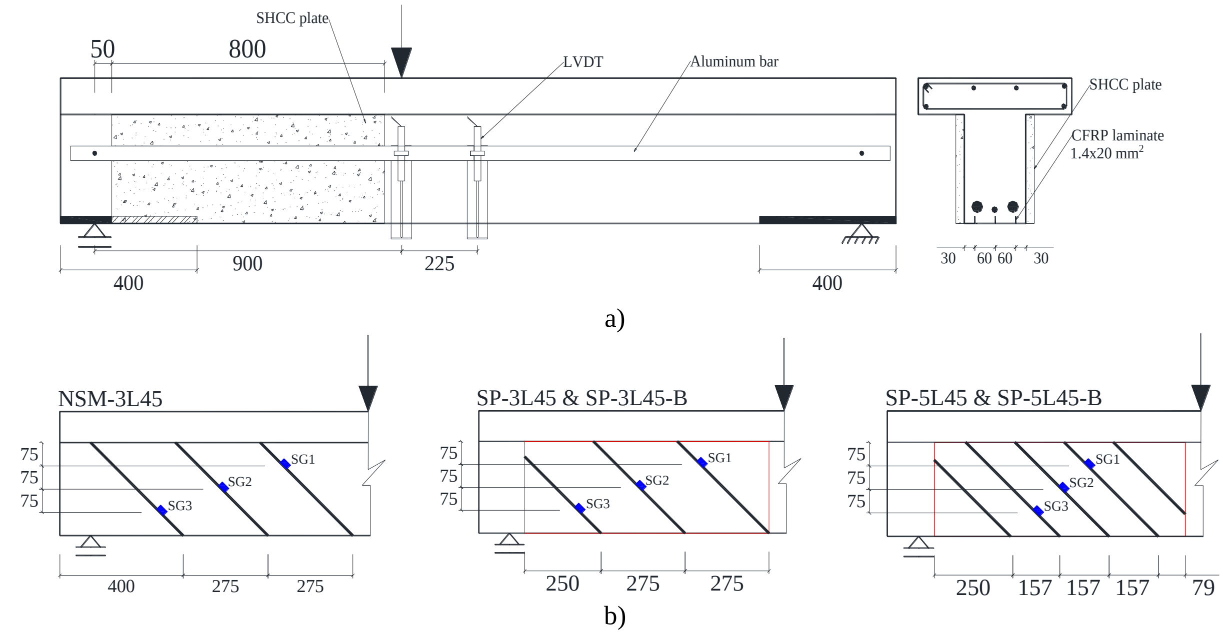

Fig. 4- Monitoring system- position of the: a) LVDTs; and b) strain gages in CFRP laminates (dimensions in mm)

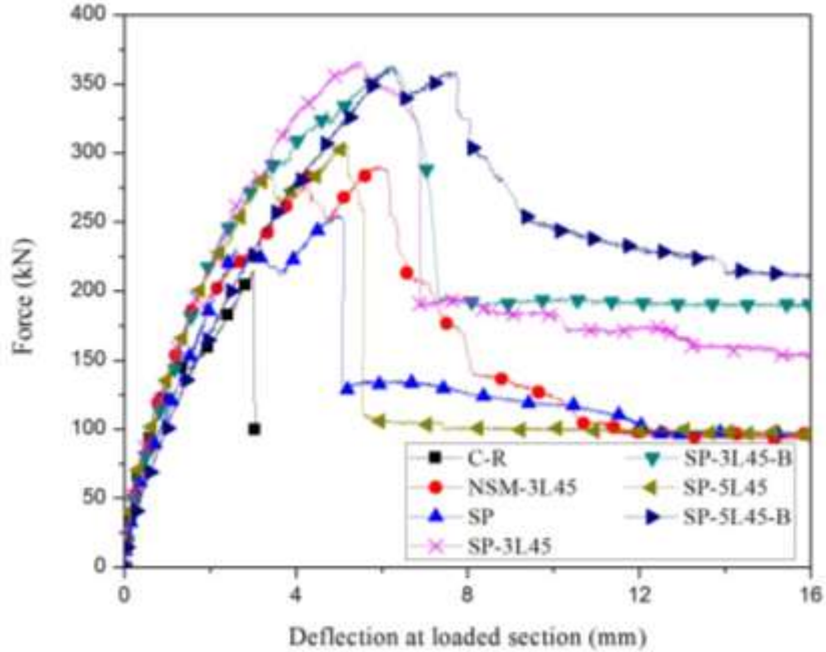
Force (kN)
Deflection at loaded section (mm)
C-R
NSM-3L45
SP
SP-3L45
SP-3L45-B
SP-5L45
SP-5L45-B

a)

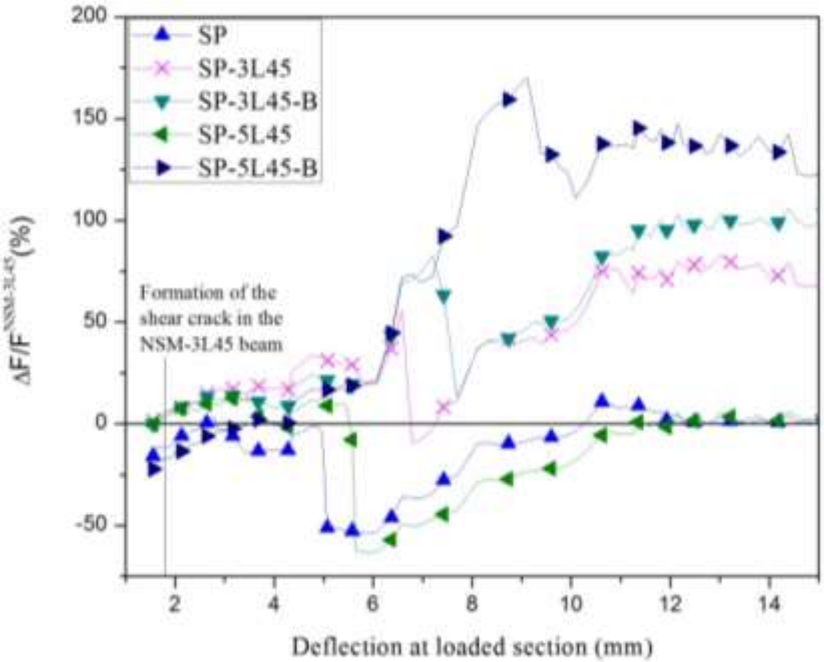
ΔF/F^NSM-3L45 (%)
Deflection at loaded section (mm)
SP
SP-3L45
SP-3L45-B
SP-5L45
SP-5L45-B
Formation of the shear crack in the NSM-3L45 beam

b)

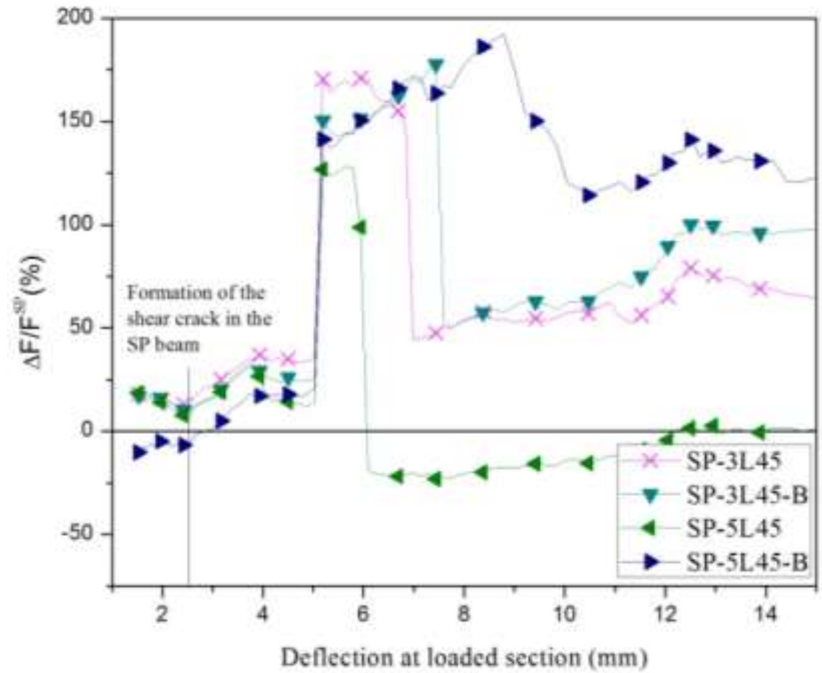

c)

Fig. 5- a) Force vs. deflection at the loaded-section, b) $\Delta F / F^{NSM-3L45}$ *vs. deflection at the loaded-section for the beams strengthened with SHCC/HCPs, and c)* $\Delta F / F^{SP}$ *vs. deflection at the loaded-section for the beams strengthened with HCPs*

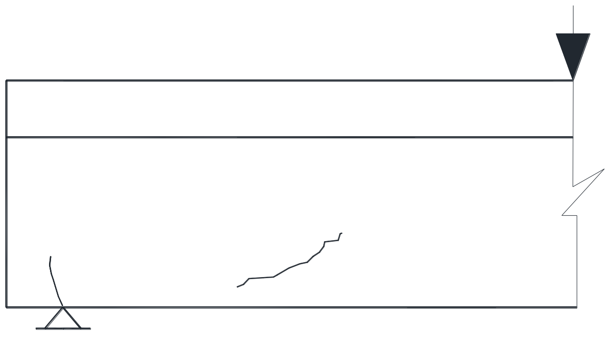

a) Crack pattern at the load level of 100 kN of the C-R beam

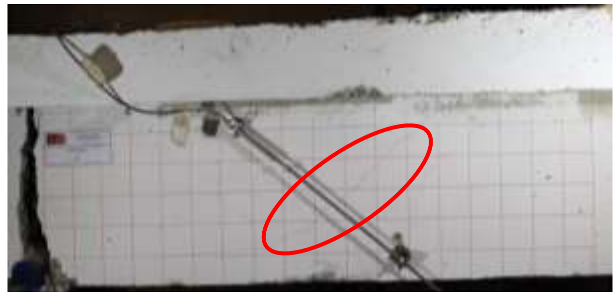

b) Crack pattern at failure load of C-R beam

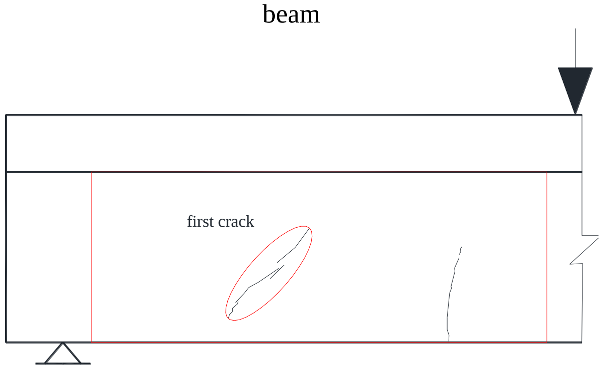

c) Crack pattern at the load level of 230 kN of the SP beam

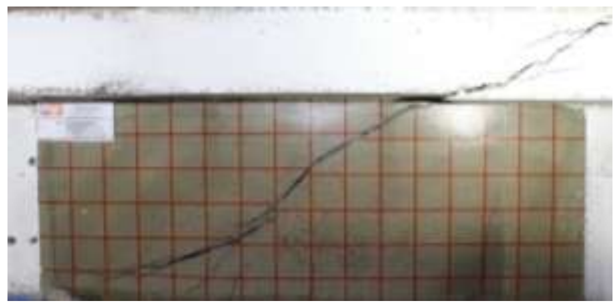

d) Final crack pattern of the SP beam

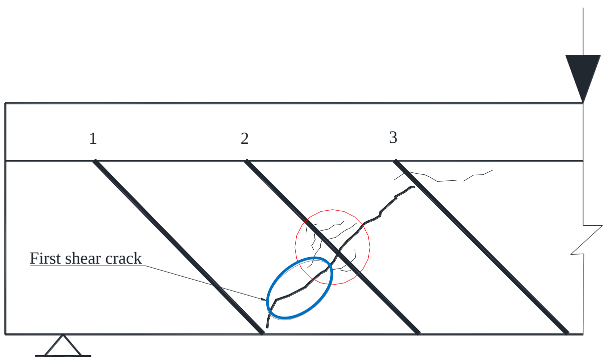

e) Crack pattern at the load level of 225 kN of the NSM-3L45 beam

f) Final crack pattern of the NSM-3L45 beam

Fig. 6 - Crack patterns and failure modes of the C-R, NSM-3L45, and SP beams

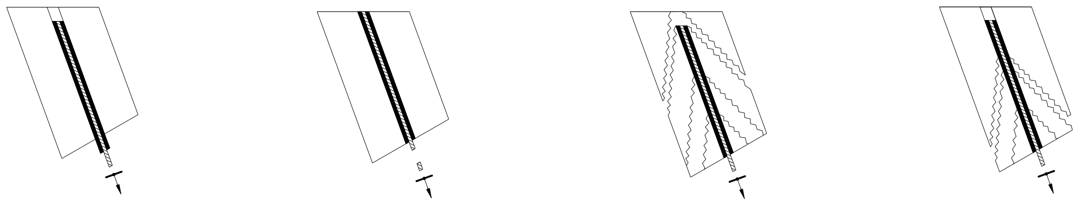

a) Debonding | b) Strip tensile rupture | c) Concrete semi-pyramidal fracture | d) Mixed shallow-semi-pyramid plus debonding

Fig. 7 - The mode of failure of an NSM CFRP laminate subjected to an imposed end slip

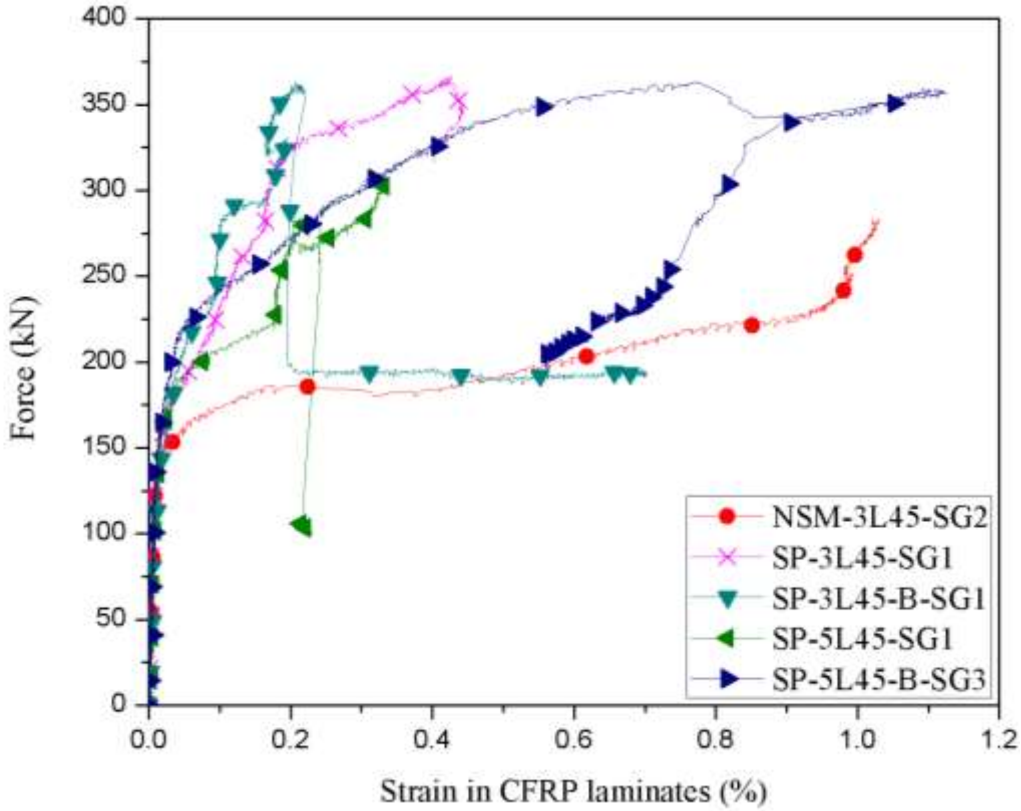

Fig. 8 - Force vs. strain in monitored laminates in SGs where the maximum strains were registered

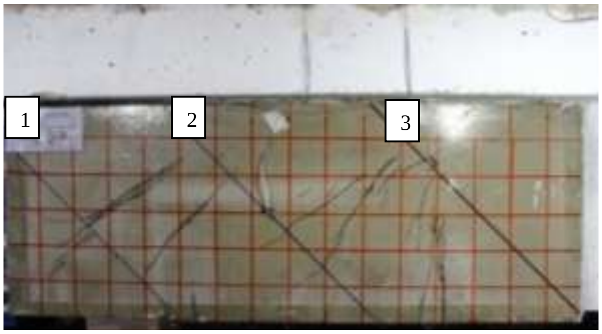

a) Crack pattern at the load level of 350kN of the SP-3L45 beam

b) *Final crack pattern of the SP-3L45 beam when HCP was peeled off after the test*

c) Local detachment of HCPs at failure load

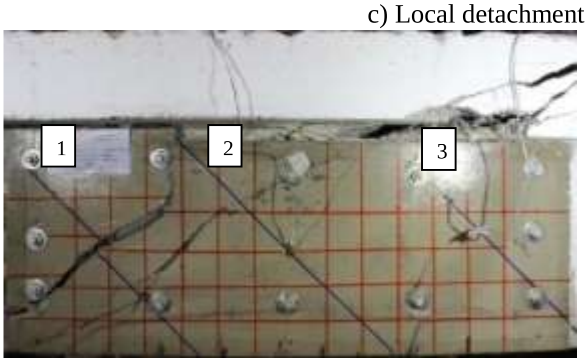

d) Final crack pattern of the SP-3L45-B beam

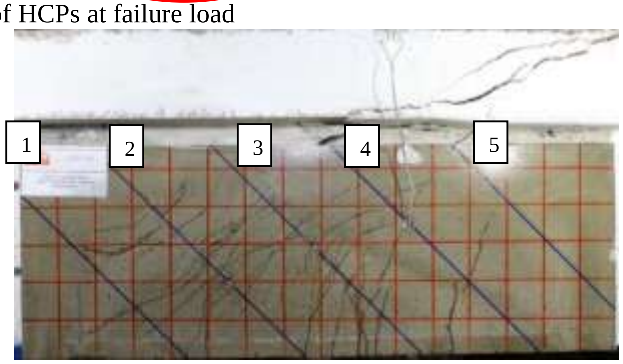

e) Final crack pattern of the SP-5L45 beam

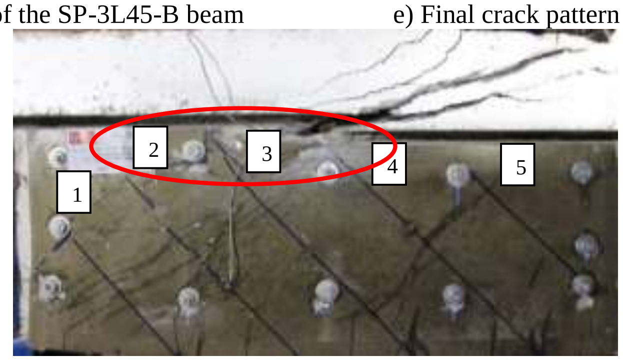

f) Final crack pattern of the SP-5L45-B beam

Fig. 9 - Crack patterns and failure modes of the strengthened beams with HCPs

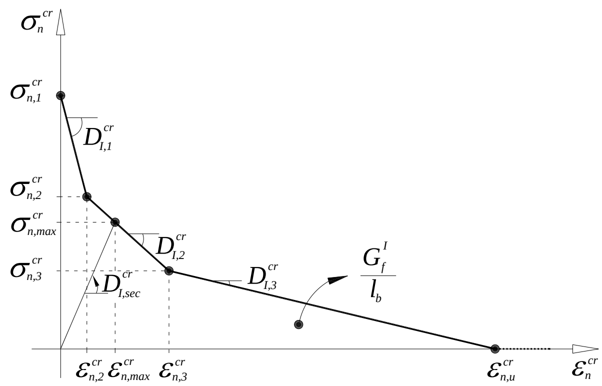

Fig. 10 - Trilinear stress-strain diagram to simulate the fracture mode I crack propagation

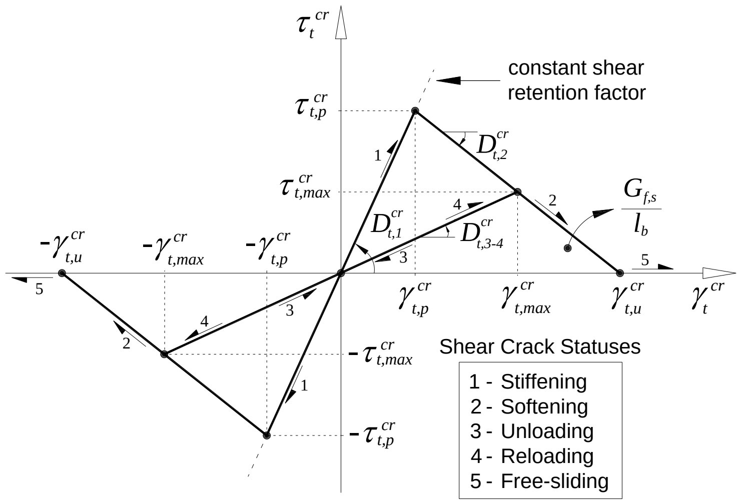

Fig. 11 - Diagrams to simulate the relationship between the crack shear stress and crack shear strain component, and possible shear crack statuses

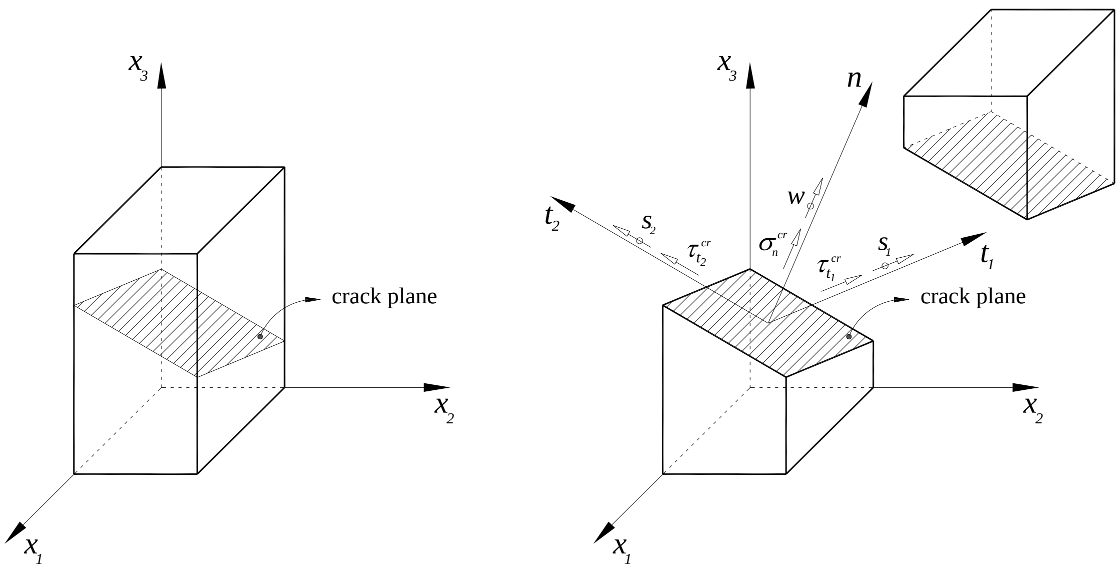

Fig. 12 - Crack stress components, displacements and local coordinate system of the crack.

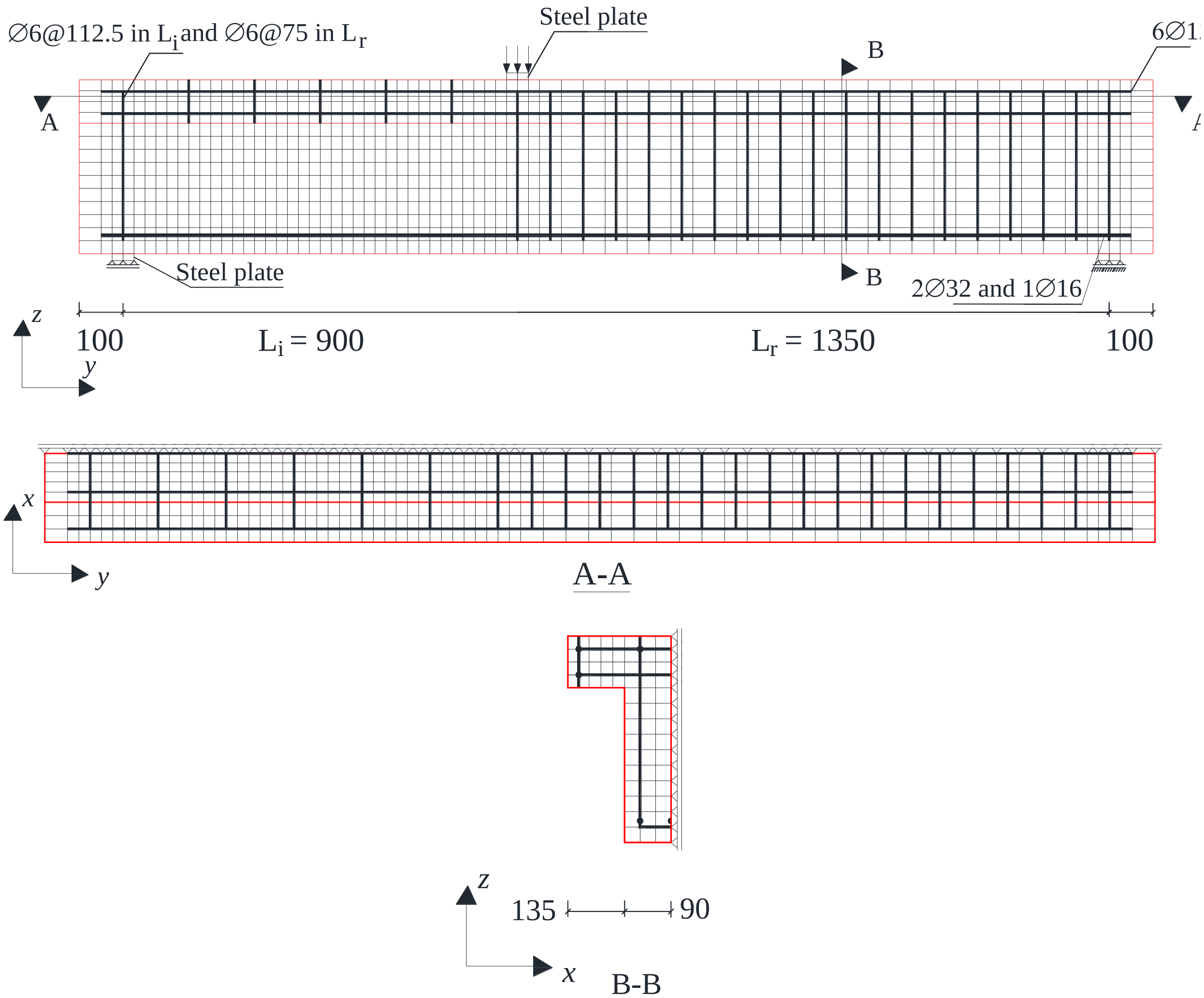

Fig. 13 - Finite element mesh of the C-R beam (dimensions in mm)

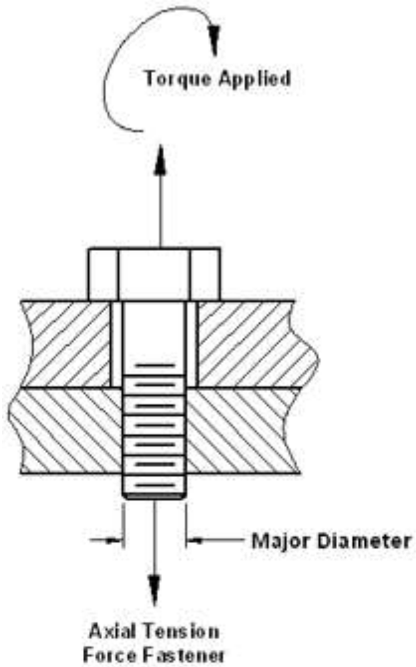

Fig. 14 – The relation between applied torque to axial tension force fastener

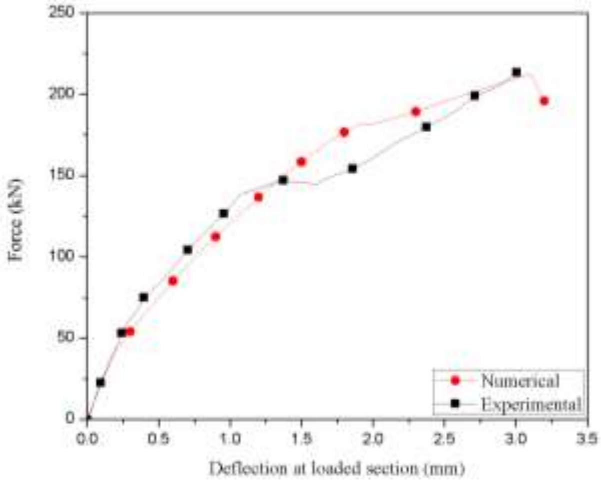

C-R

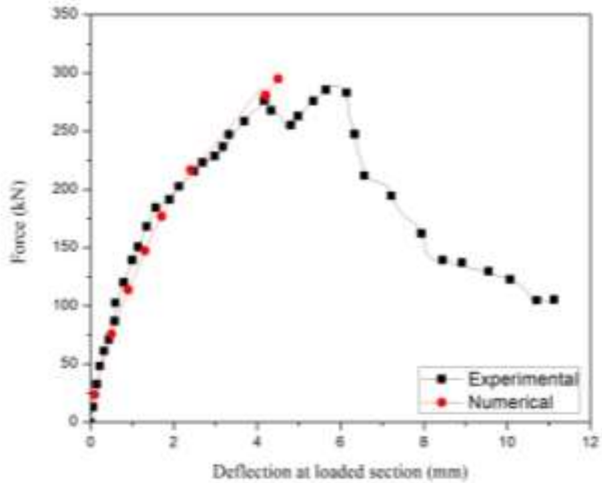

NSM-3L45

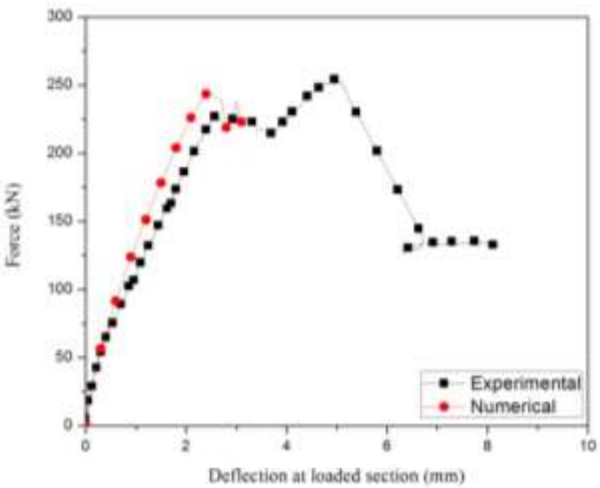

SP

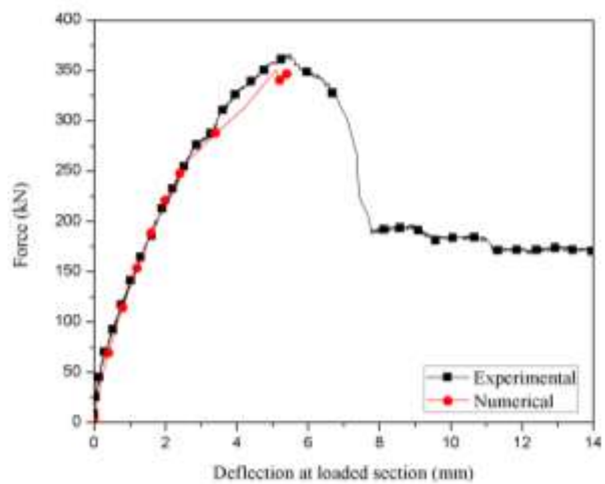

SP-3L45

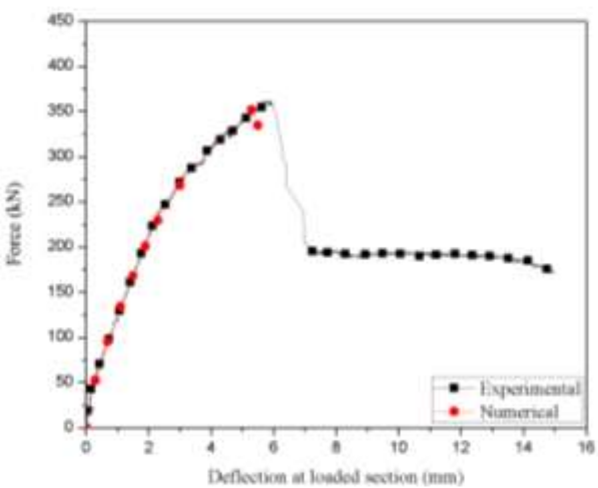

SP-3L45-B

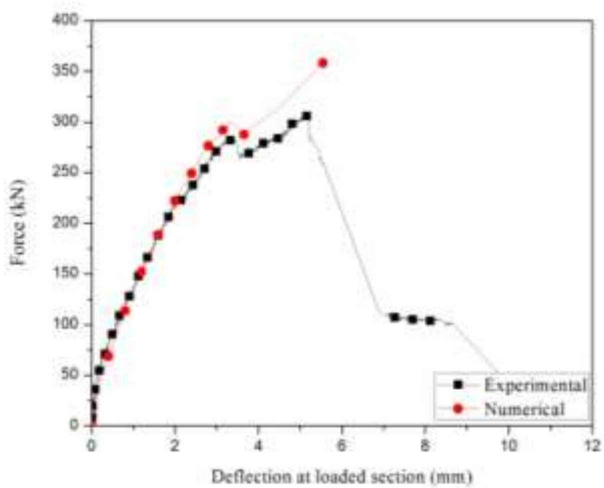

SP-5L45

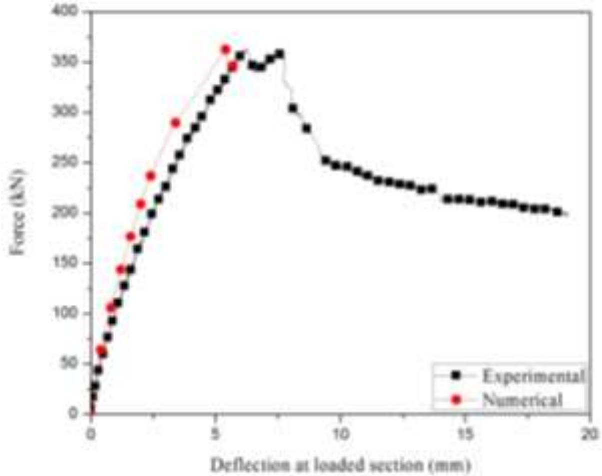

SP-5L45-B

Fig. 15 - Comparison between experimental and numerical force vs. deflection at the loaded section relationships

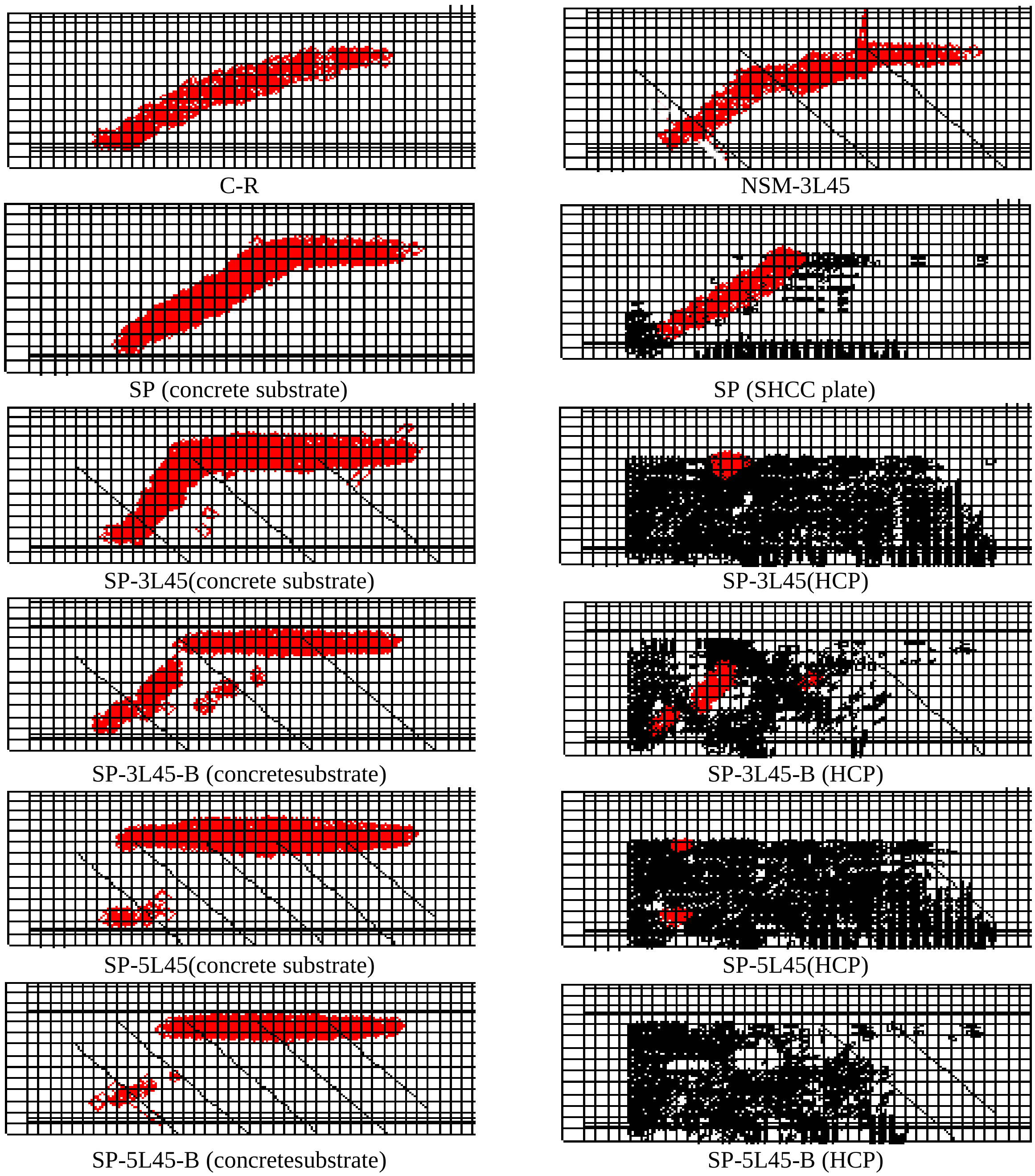

Fig. 16 - Crack patterns of the beams (in red color: crack completely open; in black color: crack in the opening process)

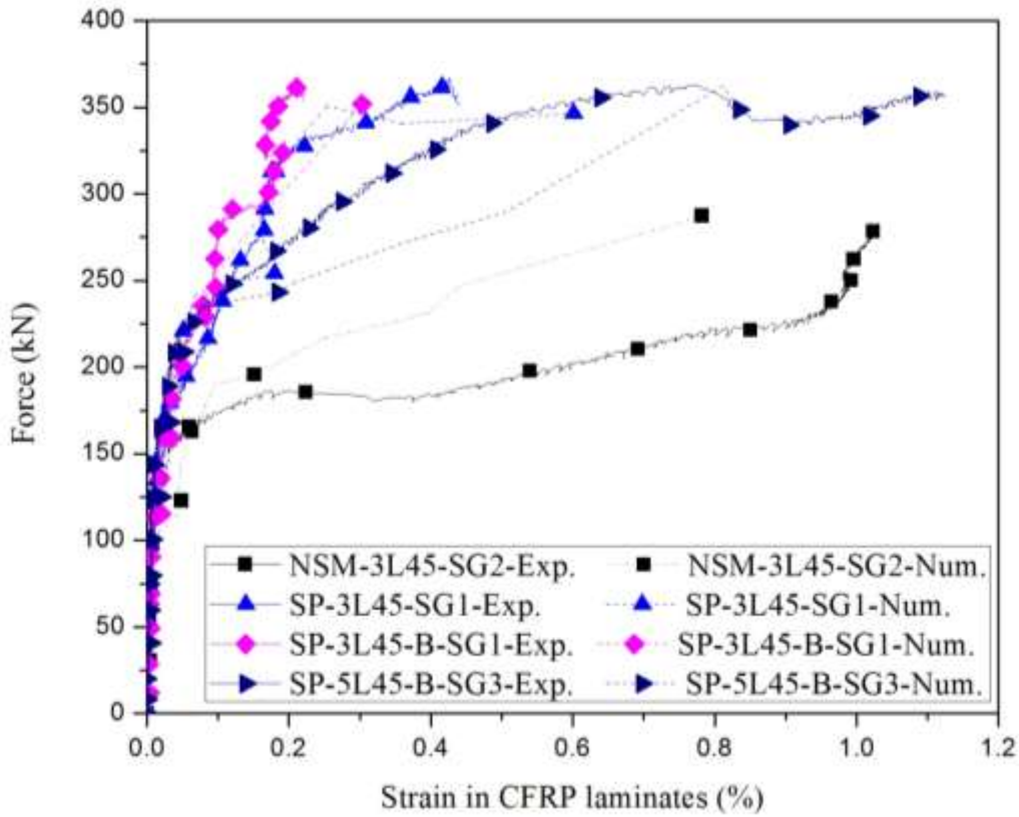

Fig. 17 - Comparison between experimental and numerical force vs. strains in the CFRP laminates

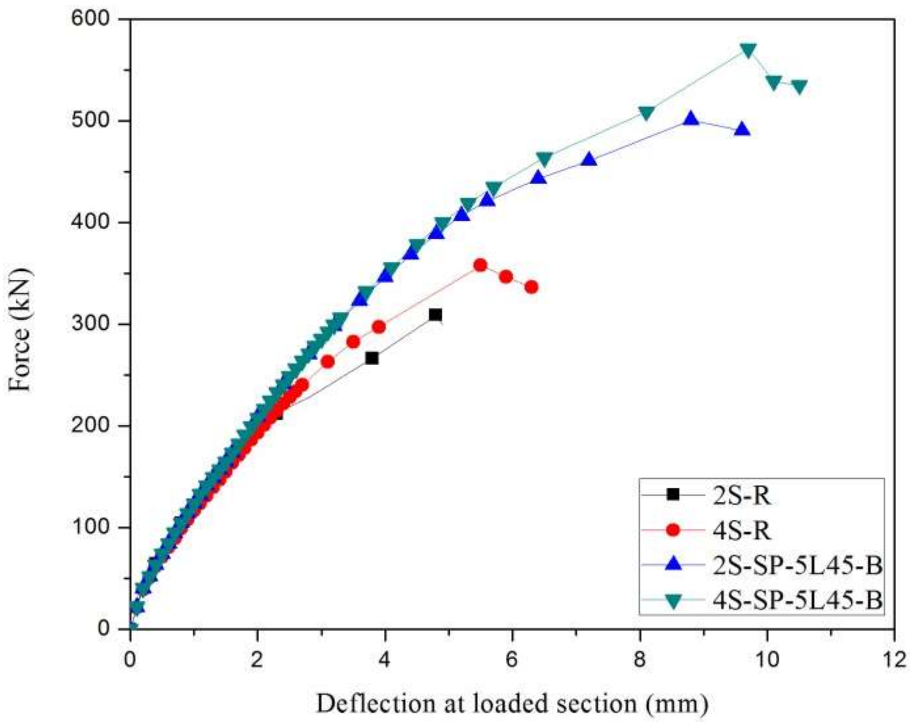

Fig. 18 – Influence of the reinforcement ratio of existing steel stirrups on the load carrying capacity of HCP strengthened beams

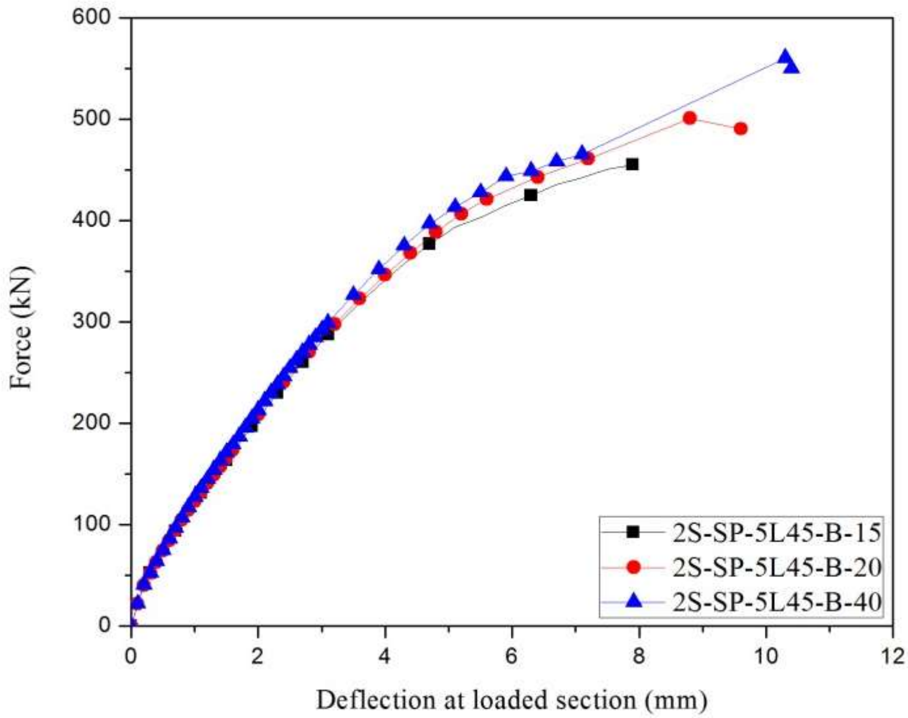

Fig. 19 – Influence of thickness of HCPs on the load carrying capacity and ultimate deflection

LIST OF TABLE CAPTIONS

Table 1- Shear strengthening/reinforcement in the monitored shear span of the tested beams

Beam designation	*Shear strengthening/reinforcement configuration*	*Quantity*	*Connection of the SHCC/HCP to substrate*	*Percentage of CFRP laminates (%)*	*Spacing, s_f (mm)*
C-R	-	-	-	-	-
SP	SHCC Plates	20 mm thickness of SHCC	Adhesive	-	-
NSM-3L45	NSM CFRP laminates of 1.4×10 mm^2 cross section	2×3CFRP laminates	-	0.08	275
SP-3L45	HCPs (20 mm thickness of SHCC reinforced with CFRP laminates of 1.4×10 mm^2 cross section)	2×3CFRP laminates	Adhesive	0.08	275
SP-5L45		2×5CFRP laminates		0.14	157
SP-3L45-B	HCPs (20 mm thickness of SHCC reinforced with CFRP laminates of 1.4×10 mm^2 cross section)	2×3CFRP laminates	Adhesive and mechanical anchors	0.08	275
SP-5L45-B		2×5CFRP laminates		0.14	157

Table 2 – Material properties

Property	*Concrete*	*CFRP laminate*	*SHCC series B*
Compressive strength (MPa)	*33.0*	-	*32.0*
Tensile strength (MPa)	-	*2620*	-
Elasticity modulus (GPa)	-	*150*	-
Maximum strain (%)	-	*1.75*	-
Tensile stress at crack initiation (MPa)	-	-	*2.5*
Tensile strength (MPa)	-	-	*3.4*
Tensile strain at tensile strength (%)	-	-	*1.3*

Table 3- material properties of the steel bars

Property	ϕ 6	ϕ 12	ϕ 16	ϕ 32
f_{sym} (N/mm^2)	500	490	470	625
f_{sum} (N/mm^2)	595	590	565	905
E_{sm} (N/mm^2)	217	196	181	208

Table 4 - Relevant results in terms of load and deflection capacity

Beam designation	$F_{\max}$ *(kN)*	*Deflection at loaded section* Δ_u *(mm)*	*Shear resistance (kN)*	$(\frac{\Delta F^{NSM-3L45}}{F^{NSM-3L45}})_{\max}$ *(%)*	$(\frac{\Delta F^{SP}}{F^{SP}})_{\max}$ *(%)*	$\frac{\Delta F_{\max}}{F_{\max}^{SP}}$ *(%)*
C-R	214	3.0	128	-	-	
NSM-3L45	290	5.9	174	0	-	14
SP	255	5.0	153	11	0	0
SP-3L45	367	5.5	220	85	176	44
SP-3L45-B	363	6.2	218	106	178	43
SP-5L45	306	5.1	184	14	131	20
SP-5L45-B	364	6.3	218	174	196	43

Table 5- Toughness indicator of the beams

Beam designation	*Energy absorption up to the deflection at maximum load (kN.mm)*
NSM-3L45	2450
SP	2070
SP-3L45	3200
SP-3L45-B	3360
SP-5L45	2200
SP-5L45-B	3700

Table 6 - Values of the parameters of the concrete constitutive model

ν_c	E_c (N/mm^2)	f_c (N/mm^2)	f_{ct} (N/mm^2)	G_f (N/mm)	ξ_1	α_1	ξ_2	α_2	$\tau_{t,p}^{cr}$ (N/mm^2)	$G_{f,s}$ (N/mm)	β
0.19	*31381*	*33.0*	*2.1*	*0.08*	*0.005*	*0.3*	*0.1*	*0.3*	*1.1*	*0.045*	*0.6*

Table 7 - Values of the parameters of the SHCC constitutive model

ν_c	E_c (N/mm^2)	f_c (N/mm^2)	f_{ct} (N/mm^2)	G_f (N/mm)	ξ_1	α_1	ξ_2	α_2	$\tau_{t,p}^{cr}$ (N/mm^2)	$G_{f,s}$ (N/mm)	β
0.15	18420	32.0	2.5	0.41	0.98	1.18	0.99	1.0	0.9	2.5	0.5